One and two dimensional single quantum and multiple quantum NMR methodologies: tools for chiral analyses

Nilamoni Nath[1,2], *Sankeerth Hebbar*[1,2], *Uday Ramesh Prabhu*[1,2] *AND N. Suryaprakash*[2]

Abstract | It is well known that enantiomers cannot be distinguished by NMR spectroscopy unless diastereomorphic interactions are imposed. Several chiral aligning media have therefore been reported for their visualization, although extensive studies are carried out using the liquid crystal made of polypeptide poly-γ-benzyl-L-glutamate (PBLG) in organic solvent. In PBLG medium the spin systems are weakly coupled and the first order analyses of the spectra are generally possible. But due to large number of pair wise interactions of nuclear spins resulting in many degenerate transitions the ^{1}H NMR spectra are not only complex but also broad and featureless, in addition to an indistinguishable overlap of the spectra of enantiomers. This enormous loss of resolution severely hinders the analyses of proton spectra, even for spin systems with 5–6 interacting protons, thereby restricting its routine application. In this review we discuss our recently developed several one and multidimensional NMR experiments to circumvent these difficulties taking specific examples of the molecules containing a single chiral centre.

1. Introduction

Isomers are different compounds possessing same molecular formula[1]. Isomers with different bond connectivity are called constitutional isomers. The isomers having the identical bond connectivity but different orientation of their atoms in space are referred to as stereoisomers. Stereoisomers are further classified as enantiomers and diastereomers. Enantiomers are stereoisomers that are mirror images of each other but at the same time are not superimposable. They rotate the plane polarized light in the opposite directions and have been classified as *R* (rectus) and *S* (sinister). On the other hand stereoisomers which are not mirror images are called diastereomers. Molecules that are superimposable on their mirror images are called achiral. Enantiomers have generally one or more tetrahedral carbon atom having four different substituents. The rate of reaction of enantiomers with achiral molecules is same. In a chiral environment the properties of enantiomers differ. They react at different rates with other chiral reagents. The discrimination of enantiomers and the quantification of excess of one form over the other are of paramount importance in pharmaceutical industry as well as in asymmetric synthesis. The Larmor frequencies of NMR active nuclei are isochronous in an achiral medium and do not

[1]*Solid State and Structural Chemistry Unit, Indian Institute of Science, Bangalore 560012, India*
[2]*NMR Research Centre, Indian Institute of Science, Bangalore 560012, India*
nsp@nrc.iisc.ernet.in

permit their discrimination. However, in a chiral environment these frequencies are anisochronous and enantiodiscrimination is possible. Therefore, for the determination of enantiomeric purity using NMR, a chiral auxiliary is essential to convert the mixture of enantiomers into a diastereomeric mixture. The distinctly identifiable resonances of enantiomers due to their chemical shifts non-equivalence enable determination of the enantiomeric excess ratio. Three types of chiral auxiliaries[2] are routinely employed for such a purpose. Chiral lanthanide shift reagents[3,4] and chiral solvating agents (CSAs)[5,6] form diastereomeric complexes in-situ with substrate enantiomers and are used directly. On the other hand chiral derivatizing agents (CDAs)[7] can be used to create diastereoisomers prior to NMR analysis.

1.1. *Chiral liquid crystal solvent and differential ordering effect (DOE)*

It was demonstrated in 1968[8] that the NMR spectra of enantiomers dissolved in a chiral anisotropic media are not identical. Anisotropic interactions being order sensitive permit their visualization. The PBLG dissolved in a helicogenic solvent act as a weakly orienting chiral medium for visualization of enantiomers by NMR spectroscopy. It has been proved to be an efficient and convenient tool for enantiomeric excess (ee) measurement. There is an anisotropic interaction between the polypeptide helices of the PBLG and the enantiomers. This leads to substantial difference in their orientational order called differential ordering effect (DOE). The choice of the solvent is very critical[9–11] for DOE. Geometric shape recognition as well as intermolecular interactions such as H-bonding, π–π interaction, etc. is the key mechanism behind such discrimination. This differential orientation of the principal axis system of the enantiomers is schematically depicted in an excellent review[9]. The various organic helicogenic co-solvents are used to align the chiral molecules in the liquid crystal PBLG[12–14]. It is found that in such co-solvents the main chain of the synthetic homo-polypeptide adopts a rigid α-helical conformation while the glutamate side chains branches out from the main helix[15–17]. The PBLG solution exhibits liquid crystalline property only over a certain range of concentrations. In this concentration range the chiral fibers orient so as to build themselves into a macroscopic supramolecular helical structure of directors in the mesophase. In a magnetic field, the supramolecular helix unwinds and the phase displays the property of a chiral nematic. The molecular diamagnetic susceptibility anisotropy is positive ($\Delta\chi_m > 0$) and the director aligns homogeneously parallel to the static magnetic field [18, 19]. Among the co-solvents the most suitable are chloroform, dichloromethane, dioxane and THF[16,20]. The necessary requirement for co-solvents is that it should homogeneously dissolve the polypeptide in addition to preserving the α-helical structure of the polymer. Unambiguous NMR results are obtained for samples with PBLG concentration ranging between 12 to 25% by weight[9]. Reasonable amount of the solute (1–20%) by weight can be dissolved in PBLG/co-solvent mixtures without disturbing the liquid crystalline property of the solvent. The average molecular weight of PBLG plays a crucial role in determining the quality of discrimination. For the same co-solvent and PBLG concentration significant reduction in viscosity of the phase is observed as the molecular weight of the solute is reduced. This is an important point because greater the fluidity, longer the transverse relaxation time (T_2^*) and hence better is the signal-to-noise (S/N) ratio.

1.2. *The order sensitive NMR parameters employed for chiral discrimination*

The NMR spectral parameters in PBLG solvent have anisotropic contributions. These are chemical shift anisotropy ($\Delta\sigma_i$), total spin-spin coupling anisotropy (T_{ij}) and the quadrupolar splitting for nuclei with $I > 1/2$ (Q_i). T_{ij} contains two contributions: dipolar coupling (D_{i_j}) and scalar coupling (J_{i_j}). The anisotropic part of the scalar coupling also contributes to T_{ij}. These anisotropic interactions are excellent tools and are employed as indicators for chiral discrimination. It may be mentioned that for protons the anisotropic contribution of J coupling is negligible compared to the dipolar coupling.

The nuclei that are of interest in unlabeled organic chiral molecules are ^{1}H, natural abundant ^{13}C and ^{2}H. The observables that can be employed for detecting DOE are: (a) chemical shift anisotropy of different nuclei, viz., $\Delta\sigma_D$, $\Delta\sigma_H$, $\Delta\sigma_C$, (b) Total spin-spin coupling anisotropy between different type of nuclei: T_{HH}, T_{HD}, T_{DD}, T_{CC}, T_{CH}, T_{CD} and (c) quadrupolar coupling Q_i . The low natural abundance of ^{13}C and ^{2}H do not permit the detection of some of these parameters. On the basis of the relative strengths of interactions, the sensitivity of anisotropic interactions to the differential ordering effect can be broadly classified in the decreasing order as, quadrupole couplings, dipolar couplings and the chemical shift anisotropies ($Q_i > D_{ij} > \Delta\sigma_i$). Therefore, the majority of the reported work in the literature makes extensive application of ^{2}H NMR benefiting from the relatively large strengths of quadrupolar couplings

and the absence of ^{2}H–^{2}H coupling in natural abundance. Before we start the detailed discussion on the application of ^{1}H NMR for the analysis of organic molecules containing a single chiral centre, the main subject of this review, a brief discussion on the use of ^{13}C and ^{2}H detection are discussed.

2. Use of ^{13}C nuclei in natural abundance

In the one dimensional proton coupled ^{13}C experiments, chiral discrimination is achieved by the difference in the value of $\Delta\sigma_i$ of ^{13}C as well as D_{CH}. For example a methyl group displays a quartet where the separations between successive transitions are given by $T^{R/S}_{CH_3} = J_{CH_3} + 2D^{R/S}_{CH_3}$. A methylene group is a triplet with the separation between successive transitions being $T^{R/S}_{CH_2} = J_{CH_2} + 2D^{R/S}_{CH_2}$ and a methine group is a doublet $T^{R/S}_{CH} = J_{CH} + 2D^{R/S}_{CH}$. Further splitting of methyl resonances are observed due to coupling ($T^{R/S}_{CH_3\ldots CH}$) with methine proton in groups like CH_3CH. However, the value of T_{CH} and $\Delta\sigma_i$ for individual carbons being different for the *R* and *S* enantiomers chiral discrimination is feasible. The signs of $^1J_{CH}$ and $^3J_{CH}$ are known to be positive and considering that $^1D_{CH}$ and $^3D_{CH}$ are smaller than $^1J_{CH}$ and $^3J_{CH}$, in the PBLG phase the absolute signs of the dipolar couplings have been determined[10]. For the discrimination based on D_{CH} highly resolved spectrum is a pre-requisite. Hence the applicability of the proton coupled ^{13}C NMR is limited to small molecules.

One dimensional proton decoupled ^{13}C experiments are advantageous in view of easy analyses, sensitivity and greater precision in measuring enantiomeric excess. Well dispersed chemical shifts aids the assignment of resonances to chemically inequivalent ^{13}C spins. The chemical shift anisotropies of ^{13}C nuclei being small in PBLG the ^{13}C chemical shift positions are nearly equal to their isotropic ones. The couplings among natural abundant ^{13}C spins are not detected. Thus the assignment of resonances to enantiomeric carbons is pretty straightforward. Enantiomeric excess could be measured from the ratiometric analysis of the discriminated peaks. Accuracy studies on both of enantiomeric excess measurement using ^{13}C detection is generally between 5–10%[9].

3. Use of ^{2}H NMR in natural abundance

The strengths of the deuterium quadrupolar interactions being larger and most sensitive to order parameter, generally majority of the studies employ ^{2}H NMR for enantiomeric discrimination[21–24] and there is voluminous amount of data reported in the literature. ^{2}H labeled and natural abundant chiral molecules have been carried out. The employment of ^{2}H NMR in natural abundance for chiral analyses is cited in the literature as NAD-NMR. Many one and two dimensional experiments have been reported for such a purpose. It has also been pointed out that deuterium T_1 relaxation rates for solutes dissolved in PBLG are generally much lower than that of ^{13}C. Therefore, the faster acquisition of data is possible with similar signal to noise ratio. This also overcomes the tedium of isotopic enrichment for observing deuterium signals in PBLG. At natural abundance J_{DD} and D_{DD} are undetected. Therefore in ^{1}H decoupled NAD NMR spectra each nonequivalent ^{2}H sites in a molecule gives rise to independent quadrupole split doublet. In a racemic mixture of enantiomers possessing "n" chemically inequivalent deuterium sites, "$2n$" doublets are observed. Voluminous amount of information is available on the use of NADNMR and a recent review summarizes the currently available two and three dimensional experiments[25].

4. Proton NMR spectral complexity and difficulty in their analyses

The routine employment of ^{1}H detection for chiral analyses is severely hampered due to enormous loss of resolution arising from numerous short and long distance couplings experienced by each spin. The sensitivity of chemical shift anisotropy ($\Delta\sigma_i$) of proton towards differential ordering effect in PBLG is very weak and the chemical shift difference between the enantiomers is negligibly small. Thus the indistinguishable superposition of two independent ^{1}H NMR spectra from the two enantiomers for a racemic mixture is inevitable. This overlap combined with broad and featureless spectra renders the analyses of ^{1}H spectra difficult even for small molecules with five or six interacting spins. The discrimination and disentangling of this overlap is not only a pre-requisite but is also a challenging task. Thus in the literature the analyses of ^{1}H detected spectra have been described as either difficult or impossible[9] and there are very few reported studies for visualization of enantiomers using ^{1}H detection. Nevertheless, the ^{1}H detected spectra, in spite of their severe complexity when employed for big molecules, is the preferred choice for chiral molecules because of its high sensitivity, high natural abundance and enormous saving of experimental time.

As far as enantiopure molecules in PBLG are concerned, the spins are generally weakly coupled and the first order analyses of the spectra are generally possible in most of the situations. However, the basic problem is the analyses of such spectra because of too many unresolved transitions. As an example the ^{1}H NMR spectra reported in Fig. 1, for

Figure 1: From top to bottom: 500 MHz one dimensional ^{1}H spectrum of; (a) (R/S)-2-chloropropanoic acid, (b) (R/S)-3-butyn-2-ol, (c) (R/S)-propylene carbonate and (d) (R/S)-propylene oxide. The expansions of the particular regions of each spectrum and the assignment to different protons are shown.

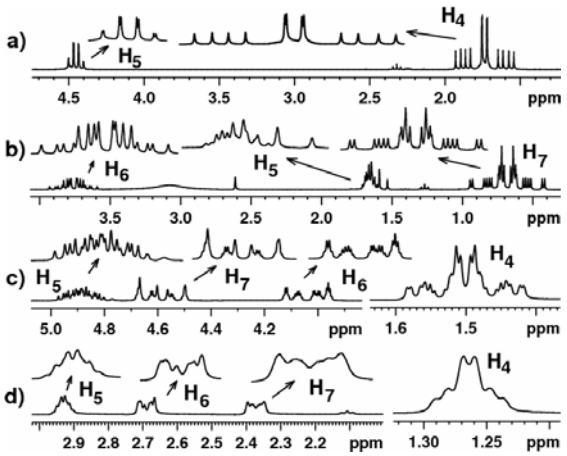

Figure 2: Racemic structures and the numbering of the interacting spins of the molecules; (A) (R/S)-2-chloropropanoic acid, (B) (R/S)-3-butyn-2-ol, (C) (R/S)-propylene carbonate and D) (R/S)-propylene oxide. The chiral centers are marked with $*$.

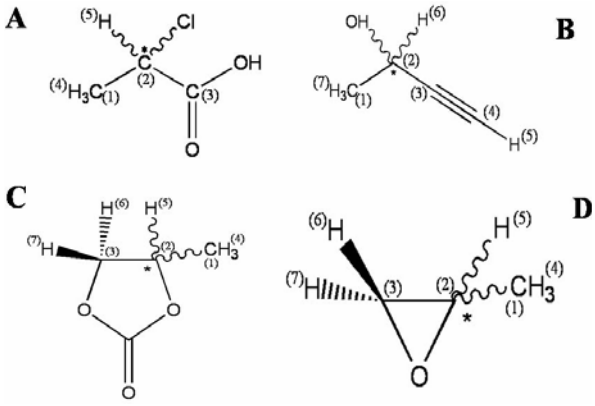

the molecules whose chemical structures and the labeling of the interacting spins are given in Fig. 2, display spectral complexity with the increasing in the number of interacting spins.

The Fig. 1A and D pertains to ^{1}H NMR spectra of (R/S)-2-chloropropanoic acid and (R/S)-propylene oxide, four and six spin systems respectively. The signal from the hydroxyl proton is broadened and does not exhibit coupling to other protons. It is clearly evident from the spectra that mere addition of two spins resulted in enormous loss of spectra resolution. Nevertheless the protons are weakly coupled and spin systems are designated as A_3X and A_3MPX respectively, where A_3 refers to methyl protons and other alphabets corresponds to different protons of the molecule.

Both the spectra are amenable for first order analyses. For the A_3X spin system unlike in isotropic systems where the methyl protons give rise to a singlet because of magnetic equivalence, in oriented systems the residual dipolar couplings results in splitting of the methyl resonance into a 1:2:1 triplet. The separation between two adjacent transitions provides $^2T_{HH}(= 3x^2D_{HH})$, where T refers to the sum of the three dipolar couplings ($^2D_{HH}$) among methyl protons and the superscript 2 refers to the proton that is two bonds away. Due to magnetic equivalence, J_{HH} does not influence the spectrum and the separation of two consecutive transitions directly provides $3 \times (2D_{HH})$. Each of these transitions is further split into doublets of equal intensity due to coupling ($^3J_{HH} + 2x^3D_{HH}$) with methine proton. Thus the six transitions observed can be visualized as two A_3 sub spectra corresponding to two spin states of X spin. One of the A_3 sub spectra corresponds to methine proton in the $|\alpha\rangle$ state and the other for the methine proton in the $|\beta\rangle$ state. Similarly the methine proton is a quartet due to its coupling with methyl protons. The first order interpretation of the A_3MPX spin system can also be carried out in an analogous manner. The methyl protons experience four different type of couplings, viz. (a) couplings among themselves ($^2T_{HH}$) leading to a triplet, (b) coupling between methyl (A_3) and methine (X-spin) proton ($^3T_{HH}$) giving a doublet for each transition of the triplet, (c) two different couplings from the two diastereomorphic methylene protons ($^4T_{HH}$) giving rise to further splitting of each transition to doublet of a doublet. Thus twenty four transitions are observed for methyl groups which can be construed as eight A_3 sub spectra corresponding to eight possible spin states of M, P and X together. The multiplicity for each M, P and X spin will be doublet of doublet of quartet. In a racemic mixture there will be an overlap of spectra from both the enantiomers.

Though the first order interpretation of the multiplicity pattern of the ^{1}H spectra of both the molecules discussed above is generally feasible, in a racemic mixture the discrimination of the spectrum for each enantiomer is a pre-requisite. Furthermore the simplification of the complex spectra by discerning the degenerate transitions is essential for the extraction of coupling information. Several novel methods have been developed in this

Figure 3: (A) The pulse sequence employed for transition selective one dimensional COSY experiment. The first pulse is the shaped pulse for excitation of selected transition and the rectangular pulse is a hard $\pi/2$ pulse. The phases of the pulses and receiver were set to x. Both the gradients G1 and G2 are 5 G/cm; (B) racemic structure of the molecule (R/S)-3-butyn-2-ol; (C) selectively excited enantiopure transition pertaining to R enantiomer, (D) 500 MHz ^{1}H spectrum of the molecule in PBLG/$CDCl_3$ mesophase at 300 K. (E) the 500 MHz ^{1}H enantiopure spectrum of the molecule corresponding to R enantiomer. The delay τ was 5 ms. The peak marked $*$ in D was excited by the SEDUCE shaped selective pulse of duration 130 ms.

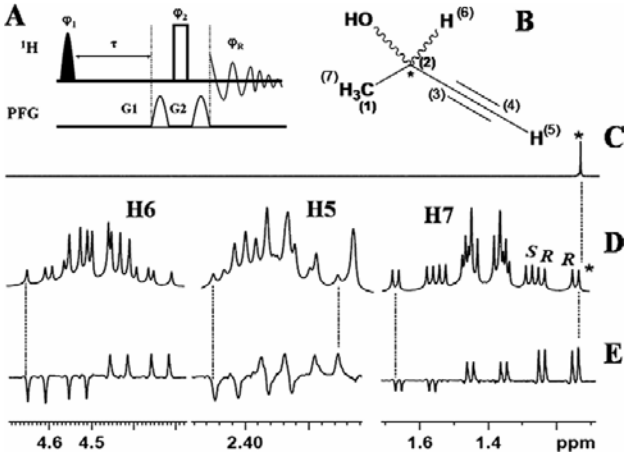

direction. All the developed experiments manipulate the spin dynamics by single and combined use of the parameters, viz. $\Delta\sigma_i$, D_{HH} or D_{CH} (with ^{13}C in natural abundance) from the proton spectrum. These methodologies can be broadly categorized as one and two dimensional techniques utilizing either single quantum or multiple quantum evolution in the indirect dimension.

5. Single quantum one dimensional experiment

As discussed earlier the ^{1}H NMR spectrum suffers from severe loss of resolution due to the presence of numerous couplings experienced by each interacting spin. This has been cited as the reason for its routine inapplicability. On the other hand in a recent study[26] the presence of residual dipolar couplings among all the protons has been demonstrated as an advantage for selective detection of spectrum of a single enantiomer. This is achieved by a simple and an elegant transition selective one dimensional (1D) ^{1}H–^{1}H correlation experiment by utilizing the pulse sequence given in Fig. 3A. The technique is demonstrated on five and six spin systems, viz. (R/S)-3-butyn-2-ol and (R/S)-propylene carbonate.

The 1D proton NMR spectrum of (R/S)-3-butyn-2-ol in PBLG/$CDCl_3$ solvent is reported in Fig. 3D. An isolated peak (marked $*$ in figure) or a pair of peaks is observed in the high field region of the methyl group of the spectrum. The isolated peak is an enantiopure transition pertaining to R enantiomer. This feature arises because of the differential intramethyl total coupling $|^2T_{HH}|$ and long distance $^nT_{HH}$ (where $^2T_{ij} = 3D_{ij}$ for equivalent spins and $^n\mathrm{T}_{ij} = J_{ij} + 2D_{ij}$ for non-equivalent spins and the superscript pertains to the number of bonds between the coupled protons) between the enantiomers. In the designed pulse scheme (Fig. 3A), a selective 90° pulse is applied on this isolated transition. Although any tip angle of the selective pulse is adequate, a 90° pulse is necessary to attain maximum signal intensity. The selectivity of the excitation of a single transition from the one dimensional spectrum is reported in Fig. 3C. Since all the protons of the molecule form a dipolar coupled network, the application of the nonselective pulse causes the transfer of magnetization from this transition to all the single quantum transitions. The delay between the pulses is chosen in such a way that it creates antiphase terms of the active spin coupled to the passive spins with highest possible intensity. A gradient ratio of 1:1 is employed in order to obviate the effect of coherences other than single quantum coherence produced by the mixing pulse. Consequent to the absence of common transition between the energy levels of both the enantiomers, this transfer of magnetization is restricted only for R enantiomer, enabling the selective detection of its single-enantiomer or enantiopure spectrum which is reported in Fig. 3E. It is clearly evident from the comparison with the 1D spectrum that all the transitions for R enantiomer are completely filtered out. The theoretical description of this concept is described in the following section.

5.1. *Polarization operator formalism for the description of the technique*

The nomenclature of this coupled protons of the molecule (R/S)-3-butyn-2-ol is A_3MX, where A_3 corresponds to methyl protons, M and X are methine and acetylenic protons respectively. The dipolar coupled A_3 spin system provides a triplet and each component of the triplet is further split into doublet of a doublet due to its couplings with M and X spins. Thus, twelve transitions are expected at A_3 chemical shift for each enantiomer. To analyze the spectral pattern and to understand the processes that occur during the pulse sequence, polarization operator formalism is employed[27]. The first selective pulse applied on the selectively excited transition creates a single quantum coherence term $A_{1+}A_{2\alpha}A_{3\alpha}M_\alpha X_\alpha$. After an appropriate delay, the application of a hard nonselective 90° pulse ensures

Figure 4: (A) The pulse sequence for further simplification of enatiopure spectrum. The phases of the pulses and receiver were x. Both the gradients G1 and G2 are 5 G/cm. The filled selective pulses were applied on the peak marked ∗ in Fig. 1D. The open shaped pulse was applied on a group of spins; (B) One dimensional spectrum of (R/S)-3-butyn-2-ol showing intramethyl coupling, $|^2T_{HH}|$ (105.2 Hz). Mixing pulse applied on methyl protons was excited by selective SEDUCE shaped pulse of duration 6.25 ms. (C) 1D spectrum of (R/S)-3-butyn-2-ol showing coupling between the methyl and acetylenic protons, $|^5T_{HH}|$ (9.8 Hz). Resonance lines of acetylenic proton was excited by SEDUCE shaped pulse of duration of 40 ms.

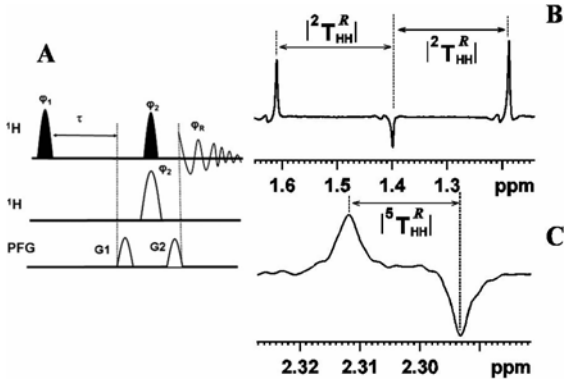

the creation of single quantum (SQ) coherences of all the spins. As an example, the SQ coherence $A_{1+}A_{2\alpha}A_{3\alpha}$ coupled to the spin state $M_\alpha X_\alpha$ gets converted to four A_{1-} SQ terms, viz.,

$$\begin{aligned} A_{1+}A_{2\alpha}A_{3\alpha}M_\alpha X_\alpha \longrightarrow \\ A_{1-}A_{2\alpha}A_{3\alpha}M_\alpha X_\alpha, \\ A_{1-}A_{2\alpha}A_{3\beta}M_\alpha X_\alpha, \\ A_{1-}A_{2\beta}A_{3\alpha}M_\alpha X_\alpha, \\ \text{and } A_{1-}A_{2\beta}A_{3\beta}M_\alpha X_\alpha \end{aligned} \quad (1)$$

The second and third terms of Eqn. (1) being degenerate have the same frequency and all the four terms give rise to a triplet. Since A_3 spins are coupled to M and X spins, each component of the triplet is further split into doublet of a doublet due to four possible spin states of M and X, viz., $|M_\alpha X_\alpha\rangle$, $|M_\alpha X_\beta\rangle$, $|M_\beta X_\alpha\rangle$ and $|M_\beta X_\beta\rangle$. Furthermore, the hard mixing pulse retains SQ coherences on M and X spins. Thus, the polarization terms for the whole process can be summarized as

$$\begin{aligned} A_{1+}A_{2\alpha}A_{3\alpha}M_\alpha X_\alpha \xrightarrow{(\pi/2)_x^{A,M,X}} \\ \frac{1}{16}A_{1-}(A_{2\alpha}+A_{2\beta})(A_{3\alpha}+A_{3\beta}) \\ \times(M_\alpha+M_\beta)(X_\alpha+X_\beta) \end{aligned} \quad (2)$$

$$\begin{aligned} \frac{i}{16}(A_{1\alpha}-A_{1\beta})(A_{2\alpha}+A_{2\beta}) \\ \times(A_{3\alpha}+A_{3\beta})M_-(X_\alpha+X_\beta) \end{aligned} \quad (3)$$

$$\begin{aligned} \frac{i}{16}(A_{1\alpha}-A_{1\beta})(A_{2\alpha}+A_{2\beta}) \\ \times(A_{3\alpha}+A_{3\beta})(M_\alpha+M_\beta)X_- \end{aligned} \quad (4)$$

The Eqns. (3) and (4) account for the appearance of the spectrum at M and X chemical shifts respectively and are doublets of quartets.

The differential intensity pattern of the spectrum for the A_3 group (Fig. 3E) could be explained by considering $A_{1+}A_{2\alpha}A_{3\alpha}$ component of single quantum coherence $A_{1+}A_{2\alpha}A_{3\alpha}M_\alpha X_\alpha$. The mixing pulse causes the creation of SQ coherences on any of the three A spins. The three such possibilities could be represented as follows,

$$A_{1+}A_{2\alpha}A_{3\alpha} \xrightarrow{(\pi/2)_x^A}$$

$$\frac{1}{8}A_{1-}(A_{2\alpha}+A_{2\beta})(A_{3\alpha}+A_{3\beta}) \quad (5)$$

$$\frac{i}{8}(A_{1\alpha}-A_{1\beta})A_{2-}(A_{3\alpha}+A_{3\beta}) \quad (6)$$

$$\frac{i}{8}(A_{1\alpha}-A_{1\beta})(A_{2\alpha}+A_{2\beta})A_{3-} \quad (7)$$

The Eqn. (5) gives a triplet with a binomial intensity of 1:2:1. The separation between the two adjacent components of the triplet provides the coupling $|^2T_{AA}|$. The Eqns. (6) and (7) are degenerate and each provides an antiphase doublet of −1:0:1 intensity with larger separation pertaining to $|2(^2T_{AA})|$. The resulting spectrum is the sum of all the sub-spectra originating from Eqns. (5), (6) and (7) and therefore, gives rise to a triplet of intensity −1:2:3. This triplet is further split into two doublets of equal intensity because of coupling of A_3 spins with M and X spins. The decrease in signal intensity from the shielded to the deshielded transition is observed in methyl group due to the application of the selective pulse on the most upfield transition. Furthermore, it could also be mentioned that the variation in this signal intensity does not have any impact on the excess measurement because the overall intensity remains invariant.

5.2. *Simplification of the selectively detected enantiopure spectrum*

Since all the protons form a coupled network, the spectrum is complex and requires further simplification. For this purpose, the pulse sequence reported in the Fig. 4A has been employed. As an example, in order to derive the coupling among the methyl protons ($A_3's$), the isolated peak marked

$*$ is selectively excited by the first pulse. After an appropriate delay, the application of the mixing pulse on the resonance lines of methyl protons ensures SQ coherence on any of the A spins. Since the pulses are acting on A_3 spins only, M and X spins are unperturbed. The processes that take place after the application of the mixing pulse can be written as

$$A_{1+}A_{2\alpha}A_{3\alpha}M_\alpha X_\alpha \rightarrow \frac{1}{8}A_{1-}(A_{2\alpha}+A_{2\beta})(A_{3\alpha}+A_{3\beta})M_\alpha X_\alpha \quad (8)$$

The spectrum is therefore a triplet which is reported in Fig. 4B. The separation between the two components of triplet gives the intramethyl coupling $|^2T_{HH}|$.

Similarly, in order to derive remote coupling between methyl protons and acetylenic proton (X), the mixing pulse is applied both on selectively excited peak marked $*$ and the resonance lines of acetylenic proton. These pulses cause transfer of coherence from this transition mediated through the coupling $|^5T_{HH}|$ (i.e. coupling between methyl protons and acetylenic proton) to the acetylenic proton. Since pulse is applied on the selected transition and X spin only, $A_{2\alpha}A_{3\beta}$ component of this SQ coherence remains unperturbed and therefore, the polarization operator that is available for detection is

$$A_{1+}A_{2\alpha}A_{3\alpha}M_\alpha X_\alpha \rightarrow \frac{1}{8}(A_{1\alpha}+A_{1\beta})A_{2\alpha}A_{3\alpha}M_\beta X_- \quad (9)$$

This indicates that the spectrum is a doublet due to $|\alpha\rangle$ and $|\beta\rangle$ spin states of A_1 spin. Fig. 4C reports a doublet pertaining to $|^5T_{HH}|$. In weakly coupled large spin systems giving isolated groups of transitions, this process of spectral simplification can be employed for deriving coupling information without resorting to numerical iterative calculations. This significantly aids the analyses of complex spectra.

For quantitative purpose, the experiment is very useful as it separates the enantiopure spectrum from the recemic mixture. Measurement of enantiomeric excess of a mixture is obtained by integrating signal area of R and S enantiomers[28]. The practical feasibility of this method for excess measurement has been carried out on a scalemic solution with 18% enrichment of S enantiomer. Difference between integral values of 1D spectrum for both enantiopure and the scalemic mixture provides the area for S enantiomer. The computed areas were employed to measure the enantiomeric excess using the Eq. (10)[25],

$$\%ee = \frac{|A_S - A_R|}{A_S + A_R} \times 100 \quad (10)$$

The ratiometric analysis provided the enantiomeric excess of S to be 18.7%. This is within the experimental error of 2%. The robustness of the method has been tested by carrying out similar studies on a scalemic mixture of (R/S)-Propylene carbonate.

6. Single quantum two dimensional techniques

6.1. *SElective ReFocusing (SERF)*

The SElective ReFocusing (SERF) experiment[28,29] compares to a standard J-resolved experimental pulse sequence in which the nonselective pulses are replaced by the selective pulses. This experiment simplifies the proton NMR spectra of enantiomers by selecting a coupling between a pair of nuclei. As an example, the methyl resonance of an enantiomer is a triplet due to dipolar couplings (D_{HH}) among methyl protons. However, their couplings to remote protons results in additional splitting of each component of the triplet and preclude the observation of any fine structure. On the other hand, if all the remote couplings to methyl protons are refocused, then two distinct triplets centered at the chemical shift for the R and S enantiomers can be visualized in the t_1 dimension. This is achieved by the application of selective π pulse on the methyl protons in the middle of t_1 dimension and retains only the couplings among the methyl protons. The central transitions of these triplets are overlapped. But the computed areas of the outer components of the triplets for R and S enantiomers provide the enantiomeric excess. In order to retain the proton–proton couplings between methyl protons and the remote proton, a biselective π pulse is applied at the centre of t_1 dimension[28].

6.1.1. *Heteronuclear selective refocusing (HETSERF)*

HETSERF experiment is analogous to the nonselective heteronuclear J-resolved experiment except that the selective π pulse is applied on particular proton resonances at the middle of indirect evolution[30]. This experiment is useful to simplify the proton coupled carbon NMR spectra of enantiomers. In this experiment, in the middle of the t_1 dimension, simultaneous application of a selective refocusing pulse on the particular group of proton(s) and a nonselective refocusing pulse on ^{13}C ensures the refocusing of all NMR interactions except the coupling between the selectively excited proton(s) and all the ^{13}C of the molecule. Thus the information content in the t_1 dimension is the couplings between the selected proton(s) and inequivalent carbons of the molecule. This simplifies

Figure 5: The pulse sequence for the selective excitation of DQ coherence of methyl protons in the molecules given in Fig. 2. The pulse phase Φ_2 is x, y, $-x$ and $-y$ with the receiver phase being x all the time. Phases of all the remaining pulses were set to x. Double quantum to single quantum coherence transfer pathway has been selected by setting the gradient ratio G_1:G_2 as 1:2. Selective pulses are SEDUCE shaped pulses.

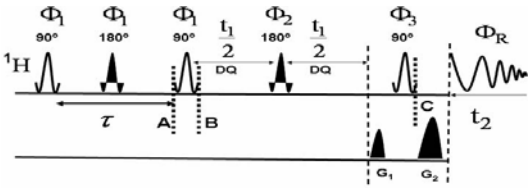

the spectral analysis. The differential values of heteronuclear couplings at different ^{13}C sites enable chiral discrimination in the t_1 dimension.

7. Double quantum two dimensional experiment

7.1. *Double quantum SElective ReFocusing (DQSERF)*

The pulse sequence for DQSERF is shown in Fig. 5. This pulse sequence developed recently[31] involves the selective DQ excitation of methyl protons. The DQ excitation corresponds to flipping of any two protons of the methyl group in the presence of its third proton. In the experiments involving the application of selective pulses, the selectively excited spins are called active spins and the remaining spins are called passive spins. An application of a selective refocusing 180° pulse on the methyl protons in the middle of the DQ dimension removes the effect of couplings from the long distance protons and retains only short distance passive coupling to methyl proton, which is not involved in DQ coherence, resulting in a doublet. The double quantum coherence evolves at the sum of the passive couplings. The sum of the two passive couplings from the passive proton being different for two enantiomers, the doublets gets separated from each other. The presence of DQ-SQ conversion pulse, unlike in SERF experiment, leads to coherence transfer from DQ coherence to SQ coherence in such a way that each cross section along SQ dimension displays a normal enantiopure one dimensional ^{1}H spectrum.

7.1.1. *Dynamics of nuclear spins in SERF and DQSERF experiments*

For theoretical understanding of the behavior of magnetization in the SERF pulse sequence a coupled A_3X spin system is considered where two different type of couplings T_{AA} $(=3D_{HH})$ and T_{AX} $(=J+2D_{HH})$ $(T_{AA} > T_{AX})$ are present (T is the sum of dipolar and scalar couplings). Although for the theoretical understanding of the pulse sequence we have assumed a weakly coupled spin system of the type A_3X, in reality the A_3 spin system cannot be treated as a weakly coupled one. The real symmetric spin functions are to be taken into account in order to analyze the spectrum.

All the three possible couplings T_{AA} in A_3 are equal. Considering the selective excitation of A spin SQ coherences and the decoupling of X spin in the t_1 dimension, by selective refocusing pulse on A spin, the SQ terms present in this dimension are

$$\frac{1}{2}[I_+^A]\frac{1}{2}[i(I_\alpha^A + I_\beta^A)]\frac{1}{2}[I_\alpha^A + I_\beta^A]. \qquad (11)$$

Thus t_1 dimension is a triplet pertaining to the four transitions $I_+^A I_\alpha^A I_\alpha^A$, $I_+^A I_\beta^A I_\alpha^A$, $I_+^A I_\alpha^A I_\beta^A$ and $I_+^A I_\beta^A I_\beta^A$ where the central two transitions are degenerate. As there is no mixing pulse between the t_1 and t_2 dimensions the spin states involved in these transitions remain unperturbed in both the dimensions. The passive coupling T_{AX} being present in the direct dimension, the transitions can be rewritten. The effective Hamiltonians, respectively in t_1 and t_2 dimensions are;

$$\bar{H} = \pi T_{I_A I_A} t_1 2 I_A^Z I_A^Z \quad \text{and}$$

$$\bar{H} = \omega_A I_A^Z + \pi T_{I_A I_A} t_1 2 I_A^Z I_A^Z + \pi T_{I_A I_X} t_1 2 I_A^Z I_X^Z$$

Corresponding to each component of the triplet in the t_1 dimension the direct dimension results in a doublet. The separation T_{AA} in t_1 dimension being different for the R and S enantiomers there is chiral discrimination visualized for the outer components of the triplets. But central transitions for the R and S enantiomers are, however, overlapped. The new feature in the modified SERF spectrum compared to that reported earlier[28] is that the remote couplings can be extracted from the direct dimension.

An A_3X spin system is considered for the analysis of DQSERF pulse sequence. It may be emphasized that the theory can be extended for different spin systems also. The selective excitation of DQ coherence of A_3 spin is assumed. The magnetization immediately after the second 90° pulse at the point B in Fig. 5 is $-2I_X^A I_Y^A$. In terms of polarization operators the terms I_X^A, I_Y^A, E^A and E^X are written as:

$$I_X^A = \frac{1}{2}(I_+^A + I_-^A), \quad I_Y^A = \frac{1}{2i}(I_+^A - I_-^A),$$

$$E^X \equiv \frac{1}{2}(I_\alpha^X + I_\beta^X) \quad \text{and} \quad E^A \equiv \frac{1}{2}(I_\alpha^A + I_\beta^A) \qquad (12)$$

Using the above operators, the MQ terms $(I_X^A I_Y^A + I_Y^A I_X^A)E^A E^X$ are written as:

$$\frac{1}{2i}(I_+^A I_+^A - I_+^A I_-^A + I_-^A I_+^A - I_-^A I_-^A) \frac{1}{2}(I_\alpha^A + I_\beta^A)\frac{1}{2}(I_\alpha^X + I_\beta^X) \quad (13)$$

However, the term $\frac{1}{2}(I_\alpha^X + I_\beta^X)$ must be neglected in the DQ dimension as the selective refocusing pulse on A spin decouples X spin.

Thus $\frac{1}{2i}(I_+^A I_+^A - I_+^A I_-^A + I_-^A I_+^A - I_-^A I_-^A)\frac{1}{2}(I_\alpha^A + I_\beta^A)$ is the only term required to be analyzed in the t_1 dimension. The first term $I_+^A I_+^A \frac{1}{2}(I_\alpha^A + I_\beta^A)$ of the above equation has a coherence order $p = 2$. This is a doublet in the DQ dimension with doublet separation $2T_{AA}$. This term is converted into SQ coherence by the last 90° pulse of the sequence at the point C. The DQ transition corresponding to $|\alpha\rangle$ state of passive spin A. The DQ–SQ transformation is written as:

$$\frac{1}{2i}(I_+^A I_+^A)\frac{1}{2}(I_\alpha^A) \rightarrow \frac{1}{2}[I_+^A + I_-^A + i(I_\alpha^A - I_\beta^A)] \frac{1}{2}[I_+^A + I_-^A + i(I_\alpha^A - I_\beta^A)] \frac{1}{2}[I_\alpha^A + I_\beta^A + i(I_+^A - I_-^A)] \quad (14)$$

(15)

In the direct dimension, the A spin SQ coherences evolve under all the couplings T_{AA} as well as T_{AX}. Thus right hand side of Eq. (15) can be rewritten as:

$$\frac{1}{2}[I_+^A + I_-^A + i(I_\alpha^A - I_\beta^A)]\frac{1}{2}[I_+^A + I_-^A + i(I_\alpha^A - I_\beta^A)] \frac{1}{2}[I_\alpha^A + I_\beta^A + i(I_+^A - I_-^A)] \quad \frac{1}{2}(I_\alpha^X + I_\beta^X) \quad (16)$$

From Eq. (16), a SQ coherence of order $p = -1$ which is observable can be detected:

$$\frac{1}{2}[I_-^A]\frac{1}{2}[i(I_\alpha^A - I_\beta^A)]\frac{1}{2}[I_\alpha^A + I_\beta^A]\frac{1}{2}(I_\alpha^X + I_\beta^X) \quad (17)$$

Thus the overall DQ-SQ transformation can be written in simple form as:

$$\frac{1}{2i}(I_+^A I_+^A)\frac{1}{2}(I_\alpha^A) \rightarrow \frac{1}{2}[I_-^A]\frac{1}{2}[i(I_\alpha^A - I_\beta^A)] \times \frac{1}{2}[I_\alpha^A + I_\beta^A]\frac{1}{2}(I_\alpha^X + I_\beta^X) \quad (18)$$

If $T_{AA} > T_{AX}$, the frequency modulation of this leads to a doublet of a triplet.

Similarly for the DQ transition corresponding to $|\beta\rangle$ state of passive spin X we get

$$\frac{1}{2i}(I_+^A I_+^A)\frac{1}{2}(I_\beta^A) \rightarrow \frac{1}{2}[I_-^A]\frac{1}{2}[i(I_\alpha^A - I_\beta^A)] \times \frac{1}{2}[I_\alpha^A + I_\beta^A]\frac{1}{2}(I_\alpha^X + I_\beta^X) \quad (19)$$

which also displays a doublet of a triplet. Thus the same multiplicity i.e. doublet of a triplet in SQ dimension is repeated in both the cross sections corresponding to the two DQ transitions in the t_1 dimension. The theoretical approach is valid for any molecule so long as there is an isolated CH_3 group for selective DQ excitation, viz., and (R/S)-2-chloropropanoic acid, (R/S)-3-butyn-2-ol, (R/S) propylene carbonate and (R/S) propylene oxide, etc whose structures are reported in Fig. 2.

7.1.2. *Analyses of SERF and DQ-SERF spectra of an A_3 X and A_3 MPX spin systems*

The SERF and DQSERF spectra pertaining to spin systems A_3X and A_3MPX, viz., (R/S)-2-chloropropanoic acid and (R/S)-β-butyrolactone are given in Figs. 6 and 7 respectively. In SERF experiment, the three transitions for the dipolar coupled A_3 spin system in the t_1 dimension can be calculated as $-T_{AA}$, 0, $+T_{AA}$. Since the central transition from the methyl protons at the middle of the spectrum does not evolve, it is always at zero frequency. The frequencies in the t_2 dimension appear at $\omega_A - T_{AA}$, ω_A, $\omega_A + T_{AA}$. The absence of mixing pulse in SERF experiment, unlike in DQ-SERF experiment, indicates that the spin states involved in the SQ transitions remain same both in t_1 and t_2 dimensions. Thus the transition at $-T_{AA}$ in t_1 dimension correlates to a transition at $\omega_A - T_{AA}$ in t_2 dimension, the transition at 0 in t_1 dimension correlates to a transition ω_A in t_2 dimension, and the transition at $+T_{AA}$ correlates to a transition at $\omega_A + T_{AA}$. Hence there is a diagonal tilt of the peaks (analogous to untilted 2D J-resolved spectrum) in such a 2D correlation matrix.

The different values of T_{AA} for the R and S enantiomers provide chiral discrimination in the t_1 dimension for the outer transitions at the frequencies $+T_{AA}^R$, $-T_{AA}^R$ and $+T_{AA}^S$, $-T_{AA}^S$. However, the central transitions at zero frequency for both R and S forms are overlapped. In molecules possessing other interacting protons the t_2 dimension is a multiplet due to the remote couplings for cross sections taken at frequencies $+T^R$, $-T^R$ for the R enantiomer and $+T^S$, $-T^S$ for the S enantiomer at these cross sections. However, the multiplets arising out of the remote couplings for both the enantiomers are overlapped

Figure 6: (A) The 500 MHz ^{1}H 2D SERF spectrum of (R/S)-2-chloropropanoic acid in the chiral liquid crystal PBLG. Peaks corresponding to the R and S enantiomers and the separations providing the values of $({}^nT_{HH})^{R/S}$ are marked. The peak marked $*$ in the F_1 dimension is an overlap of two central transitions from the two enantiomers. The peaks in the central region of 2D projection in the direct dimension, shown in the enlarged plot in the box, cannot be correlated to the R and S for any of the molecules, as the central transitions overlap in the t_1 dimension; (B) The 500 MHz methyl selective SERF spectrum of $(R/S)-\beta$-butyrolactone. The structure of the molecule is also given adjacent to the spectrum. Peak separations that provide the values of ${}^2T_{\rm HH}$ $3\times({}^2D_{\rm HH})$, ${}^3T_{\rm HH}$ for the R and S enantiomers are marked. Peaks marked $*$ in the F_1 dimension are the overlapped R and$S$ transitions that cannot be discriminated. The peaks in the central region of 2D projection in the direct dimension could not be correlated to the R and S enantiomers as the central transition from both the forms are indistinguishable in the indirect dimension. The couplings (in Hz) derivable from the separations are, $a=({}^2T_{HH})^R=36.6$, $b=({}^4T_{\rm HH})^R=2.3$, $c=({}^3T_{\rm HH})^R=11.3$ for R enantiomer and $d=({}^2T_{\rm HH})^S=16.2$, $e=({}^2T_{\rm HH})^S=16.2$, $f=({}^4T_{HH})^S=3.9$ for S enantiomer.

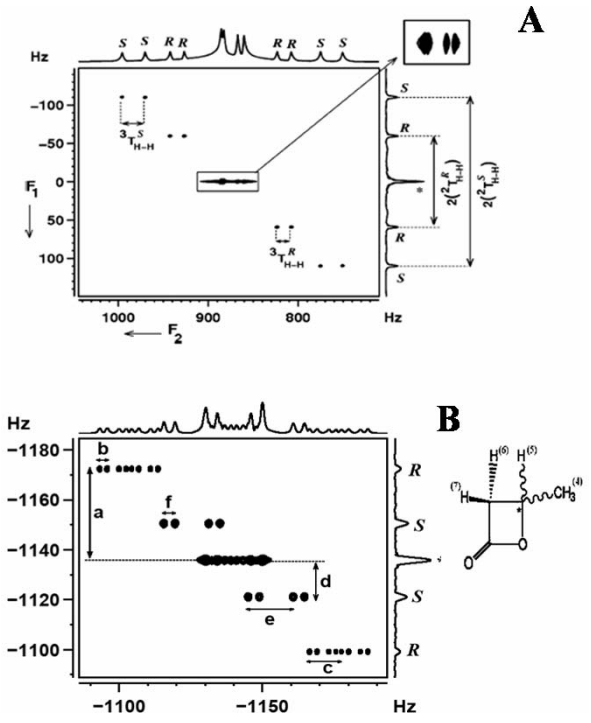

for the cross section taken along the t_2 dimension at central transition frequency of the t_1 dimension and the complete chiral discrimination is impossible in such a situation. As far as the extraction of the information is concerned it is possible even without the central transition.

The selective DQ excitation of the methyl protons and the application of a selective 180° refocusing pulse in the middle of t_1 dimension, results in an AX spin systems in the DQ dimension. However, in the SQ dimension they correspond to A_3X and A_3MPX spin system respectively. The separation of the doublet, which is $3\times({}^2D_{\rm HH})$, for each enantiomer in the DQ dimension, therefore, corresponds to the separation of the outer lines of the triplet of the SERF experiment. A distinct doublet for each enantiomer enables their unambiguous discrimination. The cross section of the spectrum taken along the SQ dimension for each transition in the DQ dimension of an enantiomer corresponds to the normal one dimensional spectrum of the methyl group. It is evident from Fig. 7 that there is a complete separation of the overlapped spectra. Each cross section provides six and twenty four transitions respectively as expected for the methyl region of A_3X and A_3MPX spin systems. The splitting patterns provide the dipolar couplings among the methyl protons (${}^2D_{\rm HH}$) and between methyl and remaining coupled protons (${}^nT_{\rm HH}$, where the superscript n refers to the proton that is n bonds away) for each enantiomer. Thus analysis of a cross section of each enantiomer taken along the SQ dimension gives all the couplings provided there is good resolution.

7.1.3. *Advantages of DQSERF over SERF*

The significant advantage of the DQ-SERF experiment is obvious when compared to the SERF experiment. In the SERF spectra shown in Fig. 6, the F_1 dimension is the X part of the AX_N and $AMPX_N$ type where N is the number of equivalent spins centered at zero chemical shift. As is evident from the Fig. 6 the central transitions from both the enantiomers are never distinguished. Further in the DQSERF spectra shown in Fig. 7, there is no central peak and the doublet for each enantiomer is well separated. In SERF spectra there is also a diagonal tilt of the doublets. This situation appears in the weakly coupled spin systems. This is very useful for the determination of the couplings to long distance protons. The cross section taken along the SQ dimension for each outer transition is a doublet with the separation ${}^nT_{\rm HH}$. On the other hand in DQSERF the cross section taken along F_2 dimension for each transition in the F_1 dimension provides the complete spectrum of the methyl group with all the short and long distance couplings.

7.1.4. *DQSERF and the measure of enantiomeric excess (ee)*

The multiple quantum excitation, consequently double quantum excitation, is non-uniform[33]. The amplitude of an excited coherence is dependent on the coupling constants. In the present case, though the nomenclature of the excited spin system is A_3 for both the enantiomers, each enantiomer has different coupling constants. To excite DQ coherence in an A_3 spin system the delay, τ, between

Figure 7: (A) The 500 MHz ^{1}H 2D DQSERF spectrum of (R/S)-2-chloropropanoic acid in the chiral liquid crystal PBLG correlating the DQ coherence of methyl protons to its SQ coherence. Peak separations providing the values of $(^nT_{\rm HH})^{R/S}$ are marked. All the peaks of 2D projection in the direct dimension could be correlated to the peaks in R and S enantiomer cross sections. The discrete vertical lines marked identify the closely resonating signals for each enantiomer in the SQ dimension. The DQ dimension provides $3\times(^2D_{HH})$ for both the enantiomers thereby enhancing the resolution for better discrimination; (B) The 500 MHz 2D DQSERF spectrum of (R/S)-β-butyrolactone in PBLG correlating the DQ coherence of methyl protons to its SQ coherence along with the corresponding projections. Peak separations which provide the values of $3\times(^2D_{HH})$, $^3T_{HH}$ for R and S enantiomers are marked. All the peaks of 2D projection in the direct dimension could be correlated to the peaks in the R and S enantiomer cross sections. The parameters that has been extracted from the separation are (in Hz), $a=(^2T_{HH})^R=36.6$, $b=(^3T_{HH})^R=11.3$, $c=(^4T_{HH})^R=2.3$ and $d=2(^2T_{HH})^R=73.2$ for R enantiomer and $g=2(^2T_{HH})^S=32.4$, $e=(^2T_{HH})^S=16.2$, $f=(^4T_{HH})^S=3.9$ for S enantiomer.

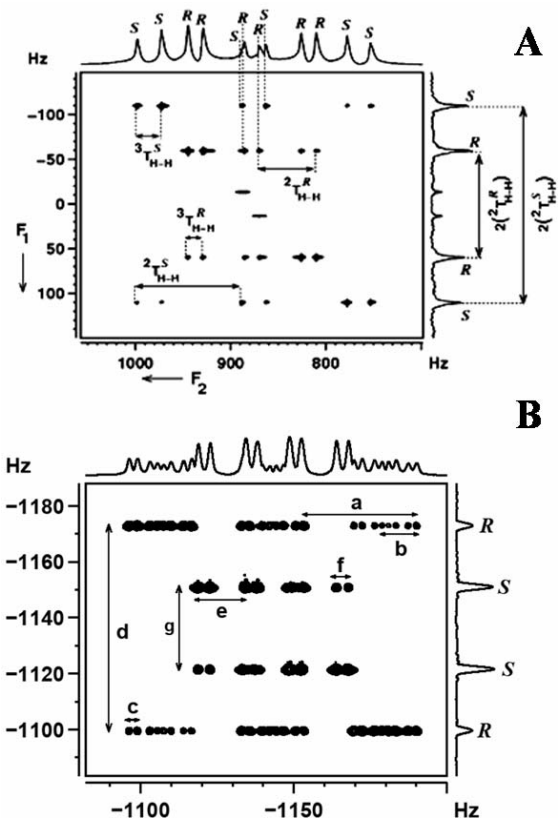

the first and the second 90° pulses should be less than $1/2(^2T_{HH})$, where $^2T_{HH}$ (which corresponds to $3(^2D_{HH})$) refers to the separation between the adjacent components of the triplets arising from proton that is two bonds away. However, the DQ excitation is maximum for $1/4(3\times^2D_{HH})$ or $1/4(^2T_{HH})$. This can be understood using the product operator formalism[34]. The terms present just before the second 90° pulse of the sequence shown in Fig. 5, for an A_3 spin system, can be written as:

$$-I_Y\cos^2\pi(^2T_{\rm HH})\tau+2I_XS_Z\sin2\pi(^2T_{\rm HH})\tau+2I_YS_ZR_Z\sin^2\pi(^2T_{\rm HH})\tau \quad (20)$$

However, the experimentally found optimum values generally do not agree with the theoretical one. One of the reasons for this is the long duration of 90° and 180° pulses and one has to consider the evolution of the magnetization during the pulses in the spin echo part of the spin selective DQ-SQ sequence. Furthermore, to derive optimum selectivity only the central region of the spectrum was considered, implying there is also a definite offset dependence of the selective pulses employed. Also the racemic mixture was made of unequal amount of R and S enantiomers and the delay, τ, had to be optimized to get the maximum signal intensity for both, which may be different from the maximum intensity of individual enantiomer. Therefore, the intensities of the DQSERF experiments are not comparable to that of normal one dimensional spectrum. Thus there are several constraints, such as; (a) the DQ excitation is maximum for $\tau=1/4(3\times^2D_{HH})$ and there is a leakage of magnetization due to the 1st and 3rd terms in Eqn. (20) for this τ value, (b) use of average τ delay, (c) the offset dependence of the shaped pulses used and (d) loss of magnetization due to zero quantum coherence. Therefore, the measurement of enantiomeric excess using the present method is tedious.

8. Single quantum two dimensional methods

8.1. *Spin selective correlation technique (Soft-COSY)*

The conventional two dimensional correlation experiment (COSY) consists of two non-selective hard pulses separated by an evolution delay. In the homonuclear spin systems, the cross peaks contain the complete multiplicity pattern. On the other hand the homonuclear COSY in the heteronuclear spin systems provide reduced cross peaks multiplicity. This is due to the fact that heteronuclear spins behave like passive spins. In spin selective excitation experiments on homonuclear spins (viz., Soft-COSY), the passive spins mimic the heteronuclei. In the spin selective correlation experiments the soft 90° pulses are applied on the chosen isolated group of coupled spins. Consequently in the two dimensional selectively excited correlation experiment there are several advantages; (a) separation of active and passive couplings in two dimensions, (b) reduced multiplicity compared to normal COSY spectrum, (c) a reduction in the experimental time by several

Figure 8: (A) The 500 MHz two dimensional correlation spectra of selectively excited methyl resonance in a racemic mixture of (R/S)-3-butyn-2-ol. The separations marked with alphabets a, b and c provide ${}^2T_{H7H7}$, ${}^3T_{H6H7}$ and ${}^5T_{H5H7}$ for R enantiomer and the separations d, e and f provide ${}^2T_{H7H7}$, ${}^3T_{H6H7}$ and ${}^5T_{H5H7}$ for S enantiomer. Peak marked * indicates the overlapped transitions from R and S. Notice the unambiguous enantiomer separation and the spectral simplification. (B) The first four cross sections for each enantiomer of Fig. 8A taken along F_2 dimension. The separations marked with alphabets a, b and c provide ${}^2T_{H7H7}$, ${}^3T_{H6H7}$ and ${}^5T_{H5H7}$ for R enantiomer and the separations d, e and f provide ${}^2T_{H7H7}$, ${}^3T_{H6H7}$ and ${}^5T_{H5H7}$ for S enantiomer. Note: The only first three cross sections for each enantiomer are sufficient for the determination of all the coupling information.

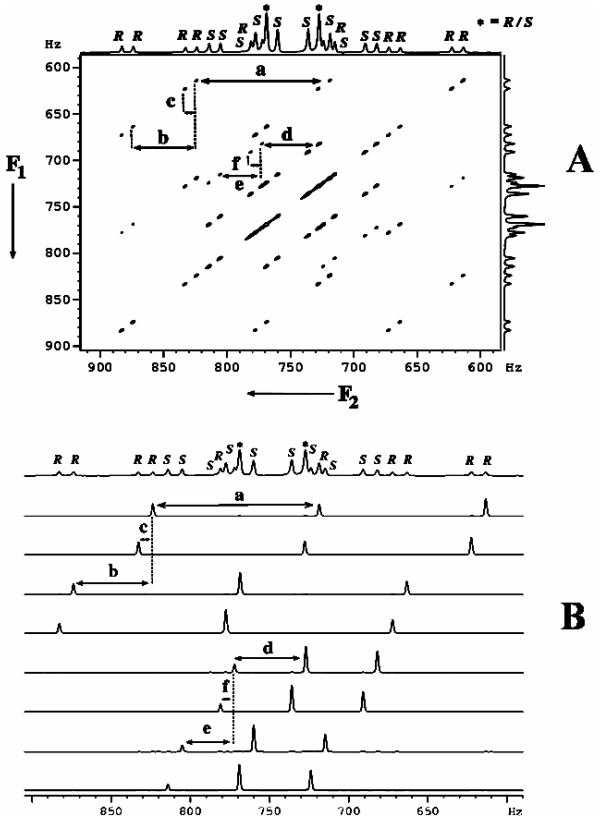

orders of magnitude and (d) higher resolution because of reduced spectral width chosen[35]. It implies that the experiment reveals several aspects of the spectrum which are otherwise not possible to derive from the normal broad and featureless one dimensional spectrum. Furthermore, there is an enhanced resolution in each cross section taken parallel to the F_2 dimension due to the fact that the states of the passive spins are not disturbed both in the F_1 and F_2 dimensions and the COSY peaks are labeled according to their spin states. As an example in a weakly coupled simple three spin system of the type AMX, the normal COSY spectrum gives sixteen cross peaks. In contrast the selectively excited COSY with a phase sensitive detection, where X is the passive spin, shows two anti-phase peaks with splitting due to active coupling displaced by a vector representing the passive splitting in both the dimensions. The F_2 dimension reveals the coupling between the active spins and the displacement of arrays in the F_1 dimension reveals the passive couplings. This is also a significant advantage as the spectrum is drastically simplified in each cross section aiding the analysis. Another interesting feature of this experiment is that the cross peak multiplicity pattern is similar to that of an E-COSY spectrum[36,37] and hence it is possible to determine the relative signs of the couplings whether the spins are scalar or dipolar coupled so long as the first order analyses of the spectra are possible. This is an excellent technique for the molecules aligned in PBLG, both for unscrambling the overlapped spectra of enantiomers and also in simplifying the spectral complexity[38]. The application of this method for the simplification of the ^{1}H NMR spectrum A_3MX and A_3MPX spin systems is discussed.

8.1.1. *Analysis of the spectrum of (R/S)-3-butyn-2-ol*

The selective methyl group excited Soft-COSY spectrum of a racemic mixture of (R/S)-3-butyn-2-ol (structure of the molecule and the proton numbering is given in Fig. 2B) is reported in Fig. 8. The active coupling is the dipolar coupling among methyl protons and the passive couplings are between methyl and the remaning two protons (5 and 6). The F_2 dimension results in twelve transitions for each enantiomer, construed as four A_3 sub spectra, which are displaced in F_1 dimension due to passive couplings. Each cross section pertains to an A_3 sub spectrum, which is a triplet and the separations of the adjacent transitions of this triplet provides $({}^2T_{H7H7})^{R/S}$. The separations marked with alphabets a, b and c provides ${}^nT_{HH}$ $(n = 2, 3$ and $5)$ for R enantiomer and the separations d, e and f provides similar information for S enantiomer. The first four cross sections taken along the F_2 dimension for each transition of an enantiomer in the F_1 dimension (Fig. 8B) depicts the complete separation of four A_3 sub spectra of both the enantiomers. It is appropriate to mention that the first three cross sections are sufficient as far as the determination of ${}^nT_{HH}$ $(n = 2, 3$ and $5)$ is concerned. The significant advantage of the spin selected correlation experiment is in spectral simplification, by separating the active and passive couplings in two dimensions. This is clearly evident from the Fig. 8.

The coupling between the passive methine and acetylenic protons numbered 5 and 6 is not reflected either in the F_1 or in the F_2 dimension in the above experiment. Another experiment with the selective

Figure 9: (A) The 500 MHz two dimensional correlation spectra of bi-selective excitation of methine (6) and acetylenic (5) resonances in a racemic mixture of (R/S)-3-butyn-2-ol, along with F_1 and F_2 projections. (B) The expanded plot of cross peaks pertaining to proton 6, marked with broken rectangle in Fig. 9A. The separations a, b and c provide respectively $^4T_{H5H6}$, $^3T_{H6H7}$ and $^4T_{H4H7}$ for R enantiomer and those marked with d, e and f provide respectively $^4T_{H5H6}$, $^3T_{H6H7}$ and $^4T_{H4H7}$ for S enantiomer. Notice the resolution achieved and the unambiguous discrimination of the enantiomers.

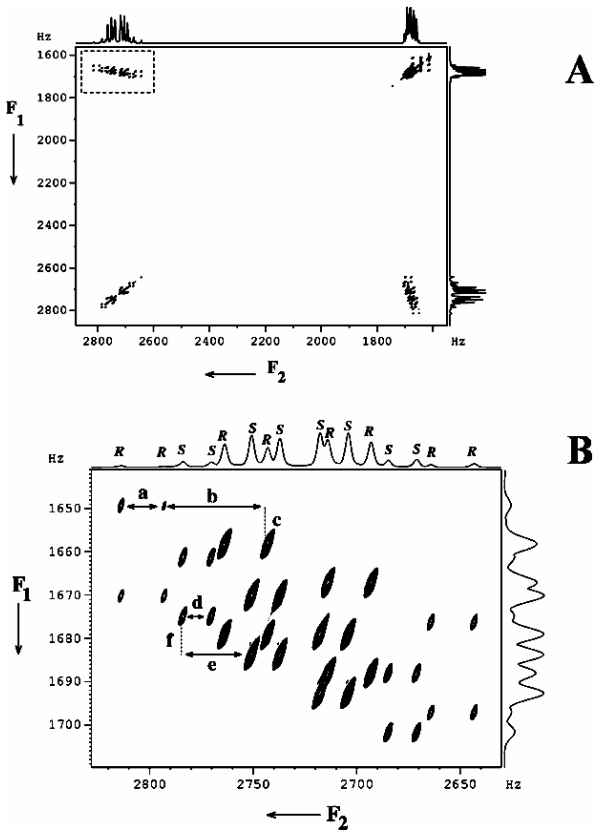

excitation of protons 5 and 6 does provide this information. The difficulty in such simultaneous excitation is their frequency separation, which is more than 1 kHz. This problem can be combated by utilizing bi-selective pulses. The bi-selective methine and acetelynic protons excited 2D spectrum is given in Fig. 9. The coupling information can be derived by the analyses of the cross peaks multiplet pattern. The set of doublets due to coupling of active spins (protons 5 and 6) along F_2 dimension are displaced in the F_1 dimension due to passive couplings with methyl protons. From the expanded plot of the cross peaks for the methine proton (6) (Fig. 9B) it is evident that the passive coupling to proton 6, $^3T_{H6H7}$ results in a quartet. Each component of the quartet are further split into a doublet by another passive coupling to proton 6, i.e., $^4T_{H5H6}$. Thus F_1 dimension gives two sets of identical quartets for each enantiomer displaced according to their coupling strengths. The separations marked with alphabets a, b and c provide $^4T_{H5H6}$, $^3T_{H7H6}$ and $^4T_{H5H7}$ for R enantiomer and the separations marked d, e and f provide similar information for S enantiomer. Thus all the couplings could be obtained by the first order analyses of the spectra without resorting to iterative analysis.

The similar 2D spin selected correlated experiments have been carried out on a scalemic mixture of (R/S)-propylene carbonate (Structure given in Fig. 2C). The coupled protons of this molecule being an A_3MPX spin system, in the selective methyl protons excited correlation experiemnt, the two non-equivalent methylene protons and the methine proton form the passive spins. The 2D spectrum then pertains to the A_3 part of A_3MPX spin system containing 24 transitions, which can be construed as eight A_3 sub spectra corresponding to eight spin states of M, P and X together, displayed in both direct and indirect dimensions, for each enantiomer. In F_2 dimension the active coupling is among the methyl protons and results in a triplet. Both F_1 and F_2 dimensions must display two sets of A_3 subspectra, one for each enantiomer with distinctly different coupling strengths enabling their discrimination. This experiment permitted the determination of only four of the seven possible independent couplings of the molecule. For the measurement of couplings among the passive protons numbered 5, 6 and 7 (M, P and X spins) another 2D correlated spectrum with selectively excited protons 5 and 7 has been carried out and is reported in Fig. 10. In this situation the methyl protons and proton 6 are passive spins. The analysis of the spectrum provides one active coupling, $^3T_{H5H7}$ and four passive couplings, $^2T_{H6H7}$, $^3T_{H5H6}$, $^3T_{H4H5}$ and $^4T_{H4H7}$. The active coupling between methine protons is obtainable along the F_2 dimension at the chemical sites of either proton numbered 6 or 7, which is a doublet of identical separation.

An expanded region of the spectrum pertaining to the cross peaks of proton 7 is reported in Fig. 10B. The active coupling of this proton with the geminal proton 6 splits its resonance into a doublet of larger separation ($^2T_{H6H7}$), which is further split into a doublet from methine proton ($^3T_{H5H7}$). Each component of the doublet of doublet is split into quartet from methyl protons ($^4T_{H4H7}$). Thus F_2 dimension provides four sets of quartets, which are displaced according to two passive couplings $^4T_{H4H7}$ and $^2T_{H6H7}$. The F_1 displacement provides two other passive couplings $^3T_{H5H6}$ and $^3T_{H4H5}$. The long distance coupling $^4T_{H4H7}$ is very small and

Figure 10: (A) The 500 MHz two dimensional correlation spectra with bi-selective excitation of protons 5 (methine) and 7 (methylene) resonances in a racemic mixture of (R/S)-propylene carbonate. (B) Expanded plot of Fig. 10A pertaining to cross peaks of proton 7 marked with broken rectangle. The separations marked with solid arrows and represented by alphabets a, b, c, d and e provide coupling information $(^3T_{H5H7})^S$, $(^2T_{H6H7})^S$, $(^4T_{H4H7})^S$, $(^3T_{H5H6})^S$ and $(^3T_{H4H5})^S$, whereas the separations marked with broken arrows and represented by alphabets f, g, h, i and j provide $(^3T_{H5H7})^R$, $(^2T_{H6H7})^R$, $(^4T_{H4H7})^R$, $(^3T_{H5H6})^R$ and $(^3T_{H4H5})^R$. Note the resolution achieved and the quartet due to long range coupling $(^4T_{H4H7})^R$ and $(^4T_{H4H7})^S$, displaced according to passive coupling in the F_1 dimension. One such quartet for each R and S enantiomers is shown by a cross line joining them.

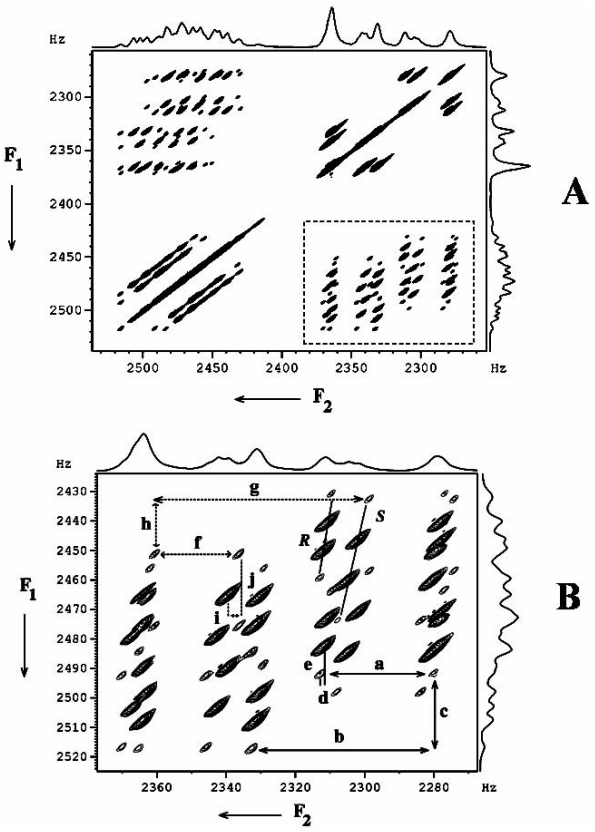

the resolution has to be exceptionally good to extract this information from the broad spectrum. One such quartet for each enantiomer is shown by joining the peaks with a tilted line. This dramatically enhanced resolution permit the measure of the coupling strength of the order of 0.6 Hz for R enantiomer. The separations marked with solid lines and represented by alphabets a, b, c, d and e respectively provide $(^3T_{H5H7})^R$, $(^2T_{H6H7})^R$, $(^4T_{H4H7})^R$, $(^3T_{H5H6})^R$ and $(^3T_{H4H5})^R$. Similarly separations marked with broken lines and represented by alphabets g, h, i, j and k respectively provides $(^3T_{H5H7})^S$, $(^2T_{H6H7})^S$, $(^4T_{H4H7})^S$, $(^3T_{H5H6})^S$ and $(^3T_{H4H5})^S$. F_1 displacement also provides $(^3T_{H5H7})^R$ and $(^3T_{H5H7})^S$. From the cross peak region of the spectrum corresponding to proton 5 similar information is obtainable. However, this experiment does not provide the precise values of $(^4T_{H4H6})^{R/S}$. Another experiment with the selective excitation of protons 6 and 7 provided the above mentioned couplings and $(^4T_{H4H6})^{R/S}$ instead of $(^4T_{H4H7})^{R/S}$. The values of $(^4T_{H4H6})^{R/S}$ and $(^4T_{H4H7})^{R/S}$ have been determined independently combining the two experiments. Thus the combination of three spin selective correlation experiments provided the complete coupling information for this molecule. These parameters would have been otherwise impossible to obtain from the broad and featureless one dimensional spectrum, demonstrating the advantage of spin selective correlation experiment.

Another additional feature of this spectrum is the determination of relative signs of the couplings from the direction of tilt of the cross sections. The information on the signs of the couplings on a similar molecule with six spins has been reported for one of the ennatiomers and the long distance couplings to diasteromeric protons have been reported to be opposite[38].

8.2. *Band selective small flip angle COSY (BASE-β-COSY)*

In the spin selective correlation technique described in the previous section, though it was possible to obtain very high resolution, several selective experiments are required to be carried out to derive all coupling information. Although, each selective experiment requires a little investment of instrument time, judicious choice of several such experiments in obtaining complete spectral information demands large instrument time. In combating this difficulty, the band selective homonuclear correlation experiment has been reported[39]. This band selection combined with small flip angle detection pulse is an invaluable experimental tool in determining very small residual dipolar couplings from the broad and featureless ^{1}H spectra of chiral molecules with minimum number of experiments and enormous saving of the instrument time.

The BASE-COSY experiment is a variant of the COSY experiment wherein a small band of frequencies is selectively excited in the t_1 dimension and correlated to the entire spectrum in the t_2 dimension[40]. The analysis of BASE-COSY spectrum is identical to normal COSY spectrum and provides couplings among all the coupled spins in a single experiment. Thus the significant advantage of BASE-COSY experiment is the zooming of the small region of the spectra in the F_1 dimension providing high

Figure 11: (A) The 500 MHz proton two dimensional BASE-COSY spectrum of (R/S)-3-butyn-2-ol with selective excitation of methyl protons (H7) along with the corresponding F_1 and F_2 projections. (B) The 500 MHz proton 2D BASE-β-COSY spectrum with selective excitation of methyl protons (H7). All the experimental and processing parameters for this spectrum are same as Fig. 11A, except that the flip angle of the second pulse is 15^0. Assignments for different protons and to R and S enantiomers are marked. (C) The expanded portion of Fig. 11B pertaining to resonance of proton H6. The active and passive couplings derivable from both F_1 and F_2 dimensions are marked. The separations providing coupling information marked with solid lines are for R enantiomer. The separations providing the coupling information are; for R enantiomer $a = {}^3T_{H6H7}$, $b = {}^4T_{H6H5}$, $c = {}^5T_{H5H7}$, $d = {}^2T_{H7H7}$ and for S enantiomer $a = {}^3T_{H6H7}$, $b = {}^4T_{H6H5}$, $c = {}^5T_{H5H7}$, $d = {}^2T_{H7H7}$. Only few of the cross sections for R and Sforms have been marked.

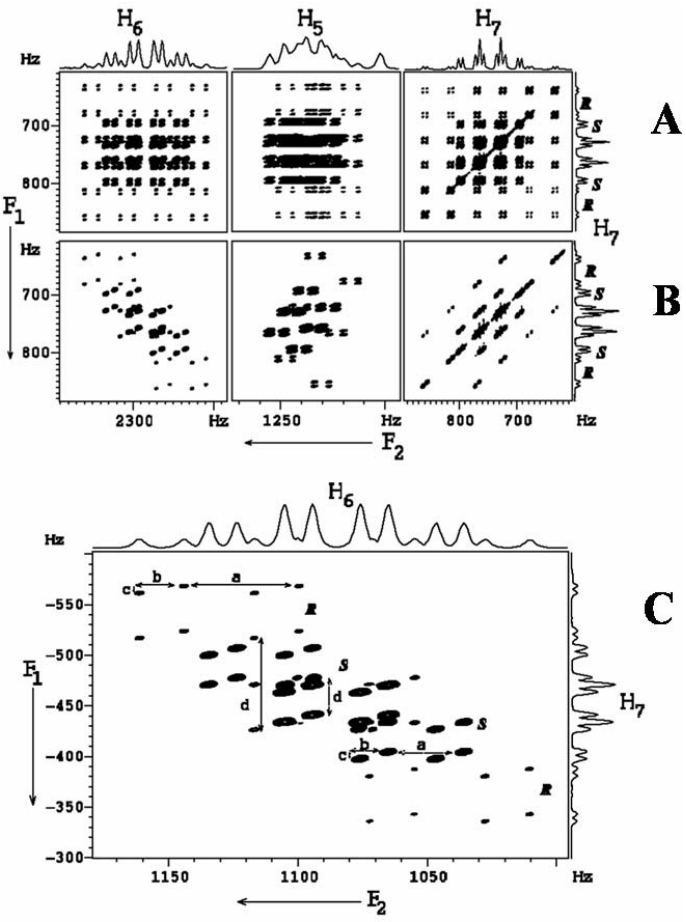

resolution. The disadvantage of BASE-COSY is that the complexity in the F_2 dimension persists and the analyses of the spectra become very tedious with too many transitions in each cross section. The problem is very severe when the number of interacting spins is very large. This problem has been combated by manipulating the dynamics of the spins. One such possibility is the use of small flip angle for the second pulse[41] in the BASE-COSY sequence which does not mix up all the energy states and is cited BASE-β-COSY. The spin states of the passive spins then remain unperturbed both in the F_1 and F_2 dimensions, resulting in the separation of active and passive couplings in the direct and indirect dimensions at the respective chemical shift positions of the entire selected band. The problem of spectral overlap due to too many transitions was therefore overcome, thereby simplifying the spectrum in each cross section. The displacement of the passive couplings in the F_1 and F_2 dimensions also enables the measurement of couplings that are less than line width. Therefore as far as the analyses and the information content is concerned, this experiment is analogous to Soft-COSY experiment[42–44], where the small region of the spectrum is selectively excited with identical source and target frequencies, giving unambiguous chiral discrimination, enhanced resolution and the separation of active and passive couplings in both the dimensions[39]. The major advantage of BASE-β-COSY over Soft-COSY is that in BASE-β-COSY there is no need of several selective experiments to determine all the spectral parameters. Furthermore, it produces an E-COSY type spectral pattern and permits the determination of relative signs of the couplings. The experimental complications in employing biselective pulses for selective excitation have also been overcome.

8.2.1. *Application of BASE-β-COSY to an A_3MX spin system*

The two dimensional BASE-COSY and BASE-β-COSY spectra of the molecule whose coupled protons form an A_3MX spin system, viz., (R/S)-3-butyn-2-ol, is reported in Fig. 11, where the source frequencies in the F_1 dimension corresponds to methyl protons and the target frequencies in the F_2 dimension is the entire spectrum. The manipulation of the spin dynamics in reducing the spectral complexity of BASE-COSY is obvious from the expanded region of the BASE-β-COSY spectrum corresponding to proton H6 (Fig. 11C). The active coupling between the excited and detected spins is determined at the respective chemical shift positions in both the dimensions. The separation providing this information is a triplet for the methyl group and doublet for the other two protons. The passive couplings with respect to the excited spins are displaced along the F_1 dimension and those with respect to the detected spin are displaced along the F_2 dimension. The active coupling $({}^3T_{H6H7})^{R/S}$ along F_1 dimension and the displacement provides passive couplings $({}^2T_{H7H7})^{R/S}$, $({}^5T_{H5H7})^{R/S}$. The passive coupling $({}^4T_{H5H6})^{R/S}$ is extracted from the displacement

Figure 12: (A) Racemic structure and the numbering of interacting spin in (R/S)-β-butyrolactone. (B) The 500 MHz one dimensional ^{1}H spectrum of (R/S)-β-butyrolactone aligned in the chiral liquid crystal PBLG. The expanded regions of each spectrum and the assignment to different protons are shown. (C) The 500 MHz proton 2D BASE-COSY spectrum with selective excitation of methyl protons (H4) along with the corresponding projections. (D) The 500 MHz proton 2D BASE-β-COSY spectrum with selective excitation of methyl protons (H4) along with the corresponding projections. All the experimental and processing parameters are identical that of as Fig. 12C, except the flip angle of the second pulse is 15°.

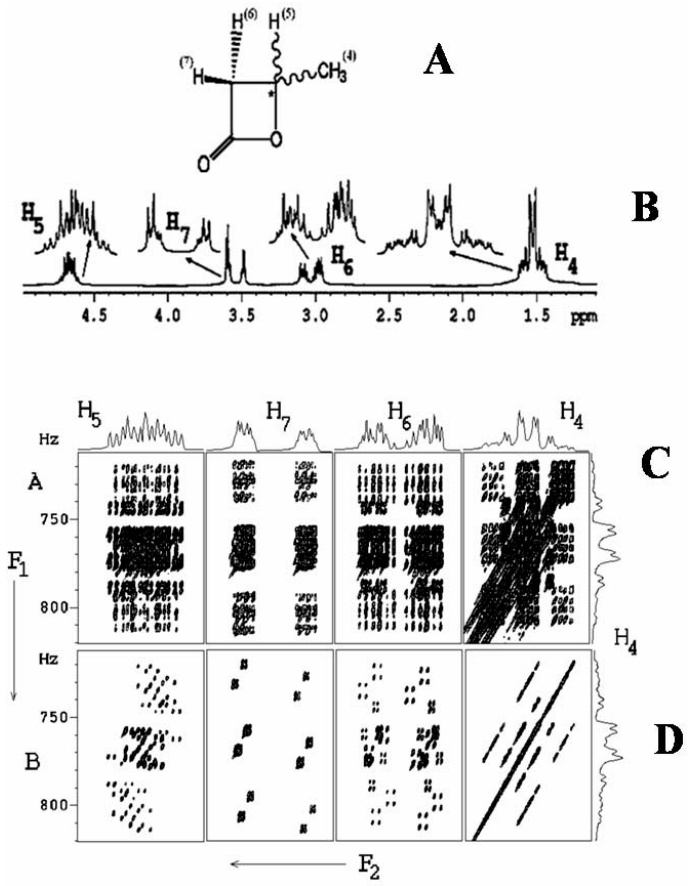

along the F_2 dimension. Thus all the couplings for both the enantiomers could be determined in a single experiment. The problem of several spin selective excitations has thus been circumvented, in addition to simplifying the analyses of the broad, featureless and complex spectra. The identical but redundant information could be obtained by the analyses of the resonances pertaining to proton H5, where the coupling along F_2 dimension is $(^3T_{H5H7})^{R/S}$ and the couplings obtainable from the displacements along F_1 and F_2 dimensions respectively are $(^2T_{H7H7})^{R/S}$, $(^5T_{H6H7})^{R/S}$ and $(^4T_{H5H7})^{R/S}$.

8.2.2. *Application of BASE-β-COSY to an A_3 MPX Spin System*

To demonstrate the application of BASE-β-COSY to a bigger molecule, (R/S)-β-butyrolactone, whose coupled protons forms an A_3MPX type spin system is chosen. The selective methyl protons excited two dimensional BASE-COSY and BASE-β-COSY spectra of this molecule are given in Fig. 12. The two non-equivalent methylene protons and the methine proton are the passive spins. In the 2D spectrum F_1 dimension pertains to the A_3 part of A_3MPX spin system containing 24 transitions. The F_2 dimension has a band of all the four groups of protons. For this molecule the analyses of the bunch of resonances pertaining to protons H6 and H5 are suffice to determine all the couplings. At the chemical shift position of proton H6, the active coupling along F_2 dimension would be $(^3T_{H4H6})^{R/S}$ and the passive couplings of all the remaining spins with proton H4 and within the methyl protons themselves, i.e, $(^2T_{H4H4})^{R/S}$, $(^3T_{H4H5})^{R/S}$ and $(^4T_{H4H7})^{R/S}$ are displaced along the F_1 dimension. On the other hand, in the F_1 dimension the active coupling is $(^3T_{H6H7})^{R/S}$. However, the passive coupling with respect to proton H6, i.e. $(^3T_{H5H6})^{R/S}$ and $(^2T_{H6H7})^{R/S}$ are displaced along F_2 dimension. Thus of the seven possible couplings could be extracted from this spectrum.

The coupling $(^3T_{H5H7})^{R/S}$ is derivable from the analysis of the resonances pertaining to proton H5. In this case the coupling along F_2 dimension is $(^3T_{H45H5})^{R/S}$ and the couplings obtainable from the displacements along F_1 dimension are $(^4T_{H4H6})^{R/S}$, $(^4T_{H4H7})^{R/S}$ and $(^4T_{H4H4})^{R/S}$. From the F_1 dimension, the passive couplings to proton H5, i.e., $(^3T_{H5H6})^{R/S}$ and $(^3T_{H5H7})^{R/S}$ can be determined. Except for $(^3T_{H5H7})^{R/S}$ all other information is redundant. The interesting point to be highlighted is that the parameters $(^4T_{H4H6})^{R/S}$ and $(^4T_{H4H7})^{R/S}$ could be obtained unambiguously from the present experiment unlike in Soft-COSY.

8.3. *z-COSY and band selected z-COSY (BASE-z-COSY) experiments*

The correlation experiments discussed in the two previous sections achieved very high resolution and also saving of the experimental time. The drawback of these correlation experiments is that the overall intensities of the cross peak multiplicities are less than diagonal peak components. Also the cross peak multiplets have absorptive line shapes while the diagonal peaks are of phase twisted in nature. For very high resolution work pure phase spectra is a dire necessity. The pure absorption mode line

Figure 13: (A) and (B) The pulse sequence respectively for z-COSY and BASE-z-COSY experiment. The duration of the 90° hard pulse in z-COSY is 11.2 μs. The small flip angle pulses, β, are 15°. The soft pulse for selective excitation in BASE-z-COSY is EUBRP-2 of duration 6.25 ms. t_z is the zero quantum suppression period. For suppression of the zero quantum coherences the swept 180° pulse employed in both the sequences are smoothed CHIRP with bandwidth of 31 kHz and of 31 ms duration. The homo-spoil gradient pulse is of strength 11 G/cm for the duration of 4 ms. The simultaneous gradient pulse of strength 4 G/cm has been applied during CHIRP. Two step phase cycling has been used to suppress the axial peaks. The phase of the first pulse and receiver has been cycled according to x, $-x$. Other pulses are of phase x unless and otherwise mentioned.

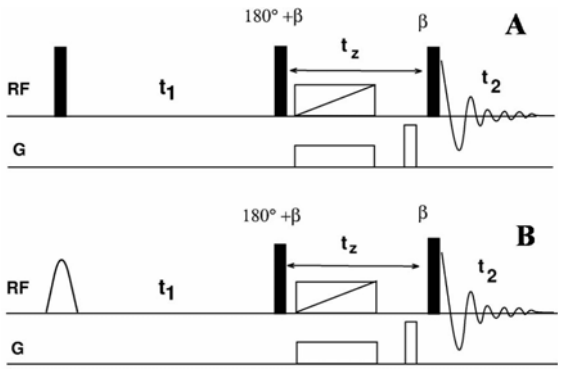

shapes provides cleaner spectrum aiding accurate chiral discrimination and the precise measure of couplings of small magnitudes hidden within the line widths, in a single experiment. In achieving good line shapes and resolution the SERFph[45] and improved SERFph[46] experiments which are the modified versions of original SERF experiment[28] have been reported. The improved SERFph pulse sequences resulted in both better line shapes and chiral discrimination but demand several single- or bi-selective excitations for obtaining complete spectral parameters, especially when the coupled spin system is big, thereby limiting the applications of these methods.

In circumventing this problem the z-filtered correlation experiment (z-COSY)[47] and a modified version of it entitled BASE-z-COSY have been employed[48]. The band selected sequence not only possess all the features of the parent z-COSY sequence but also results in enormous saving of experimental time by an order of magnitude. The methodology has been demonstrated on a chiral molecule possessing six interacting spins for obtaining complete spectral information. Also the feasibility of its application to bigger molecules of real pharmaceutical interest, (*R*/*S*)-Ibuprofen, possessing 17 interacting spins (excluding OH proton) has been explored.

The pulse sequence employed for z-COSY is given in Fig. 13[47]. It is a variant of the COSY sequence wherein both the diagonal and cross peak multiplicities have comparable intensities and both have absorption mode line shapes. The 2D data matrix has reduced multiplicity pattern due to the occurrence of the coherence transfer, during the mixing time, between the transitions that share common energy levels. z-COSY finds wide application as demonstrated in the automated analyses of the spectra by pattern recognition[49], and by using energy level connectivity information[50–53]. However, inspite of several advantages there are very few examples of the application of z-COSY technique for the analyses of the NMR spectra of bigger biomolecules[54].

8.3.1. *z-COSY and suppression of zero quantum coherence*

As depicted in Fig. 13 z-COSY is a three pulse sequence and the mixing period consists of small flip angle pulses with delay between them. This sequence yields coherence transfer between directly connected transitions. The flip angles of the pulses are governed by a compromise between sensitivity and selectivity. This is due to the fact that one has to suppress undesirable cross peaks. It is also true that z-COSY experiment is less sensitive compared to Soft-COSY and BASE-β-COSY experiments discussed in the previous sections. However, this is not a drawback when proton is detected. On the other hand, one can derive benefits from this sequence in the form cleaner spectrum obtainable in pure phase mode and with comparable intensities between cross peaks and diagonal peaks. But the inherent problem of z-COSY sequence is the presence of zero quantum coherences between the second and the third small flip angle pulses resulting in unwanted dispersive components of the spectrum. Neither the phase cycling nor the gradient suppresses the zero quantum coherences. One of the ways of discarding this unwanted coherence is to repeat the experiment with stochastic variation of delay between the pulses. This retains only the z-magnetization and suppresses all other unwanted coherences. Alternate and efficient way has been reported wherein the z-filter is modified to eliminate the zero quantum coherences in a single experiment by applying a swept frequency 180° pulse between the two small flip angle pulses with the simultaneous application of a gradient pulse[55]. In the reported work[48] Thrippleton-Keeler element has been used for the suppression of zero quantum coherences[55].

Figure 14: (A) The 500 MHz 2D z-COSY spectrum of (R/S)-propylene carbonate aligned in the solvent PBLG with suppression of zero quantum coherences, recorded at ambient temperature with corresponding F_1 and F_2 projections. Assignment of resonances to individual protons is also marked. The size of 2D data matrix is 4096×6806. Spectral widths are 2750 and 3094 Hz in F_1 and F_2 dimensions. Number of accumulations for each t_1 increment is 2. The relaxation delay is 2.0 s. The data was zero filled to 4096 and 8192 points and processed with an exponential window function. The digital resolution in F_1 and F_2 dimensions are 0.7 and 0.4 Hz respectively. The racemic structure of molecule is given as an inset in the 2D spectrum. The expansion for each proton is given in solid rectangle and is identified by an arrow. Further below each of these expansions the particular F_2 cross section denoted by an arrow is plotted to depict the pure phase character of the peaks.

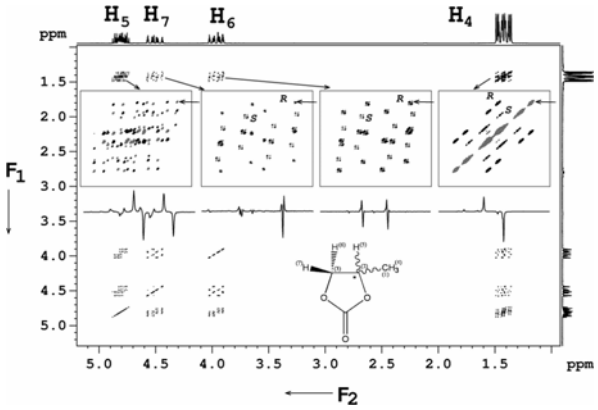

Figure 15: The 500 MHz 2D z-COSY spectrum of (R/S)-propylene carbonate with suppression of zero quantum coherences, recorded at ambient temperature and permitting the aliasing of methyl protons in the F_1 dimension. The size of 2D data matrix is 1024 × 8192. Spectral widths are 700 and 3754 Hz in F_1 and F_2 dimensions. Number of accumulations for each t_1 increment is 2. The relaxation delay is 10.0 s. The data was zero filled to 2048 and 16384 points and processed without any window function. The digital resolution in F_1 and F_2 dimensions are 0.7 and 0.4 Hz respectively. Given in the inset of a solid rectangle are the F_1 projections of (A) z-COSY spectrum, (B) expanded portion of A marked with broken rectangle and C) expanded portion with aliased z-COSY.

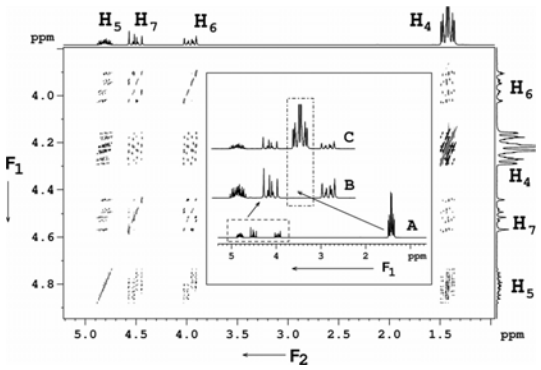

The zero quantum coherences suppressed z-COSY spectrum of (R/S)-propylene carbonate is reported in Fig. 14[48]. The reduced multiplicity pattern and the pure phase spectrum with very high resolution are clearly evident from the expanded regions of cross peak multiplet pattern. As expected the differential ordering effect resulted in a distinct and identifiable coupling pattern for each enantiomer, enabling their precise discrimination, which is marked for selected peaks. The experiment also provides the separation of active and passive couplings in the direct and indirect dimensions at the respective chemical shift positions of each proton. The evidence for the pure phase character is demonstrated in the particular F_2 cross section plotted below the 2D spectrum of Fig. 14. Although the first 90° pulse in the z-COSY sequence is with a non-selective excitation, the cross peak multiplicity pattern is identical to BASE-β-COSY spectrum. This implies that all the couplings are derivable for both the enantiomers by a single experiment. The separations providing $({}^{n}T_{HH})^{R/S}$ are identical to those reported for BASE-β-COSY spectrum[39].

The large size of the 2D data matrix is the major drawback of the z-COSY experiment. The number of increments in the t_1 dimension should be large enough for obtaining the spectrum with acceptable resolution. This puts heavy demand on the instrument time requirement. One of the ways of circumventing this constraint is aliasing the part of the spectrum in the indirect dimension[56,57]. The methyl peak aliased spectrum of (R/S)-propylene carbonate is reported in Fig. 15. In the inset of the Fig. 15 is given the full spectrum, with the expansion of the region marked with broken rectangle. This is compared with identical expanded part of the aliased spectrum. The transitions of the methyl group are well isolated and this method resulted in considerable saving of the instrument time. This experiment worked very well on a specific example where the aliasing did not result any overlap with other regions of the spectrum. But in realistic situations the technique of aliasing lacks wide generality and versatility.

In getting around the problem of time constraint, a band selective version of z-COSY, entitled as BASE-z-COSY (Fig. 13B) has been reported, which combats both resolution and experimental time constraints in a single experiment. The major difference in the new experiment is the initial soft 90° pulse used for selective excitation of particular band of frequencies which is then correlated to the entire frequency range of all the coupled spins during the t_2 period. As far as the remaining part of the sequence is concerned there is a complete overlap with the conventional z-COSY sequence.

Figure 16: (A) The 500 MHz 2D methyl group selected BASE-z-COSY spectrum of (R/S)-propylene carbonate in the solvent PBLG; The size of 2D data matrix is 512×8192. Spectral widths are 280 and 4562 Hz in F_1 and F_2 dimensions. Number of accumulations for each t_1 increment is 2. The relaxation delay is 2 s. The data was zero filled to 1024 and 16384 points and processed without any window function. The digital resolution in F_1 and F_2 dimensions are 0.5 Hz in both dimensions. (B) The BASE-β-COSY spectrum of (R/S)-propylene carbonate in the solvent PBLG recorded in phase sensitive mode using TPPI. All experimental and processing parameters are same as A, except for the number of accumulations for each t_1 point, which is 4. C) All experimental parameters are identical to that given in A except for the spectrum is presented in magnitude mode. The one dimensional spectra shown below A, B and C are the particular F_2 cross sections depicted by the arrows. Note the pure phase spectrum in A and phase distorted spectrum in B. It is clearly evident that the lines are narrower in A.

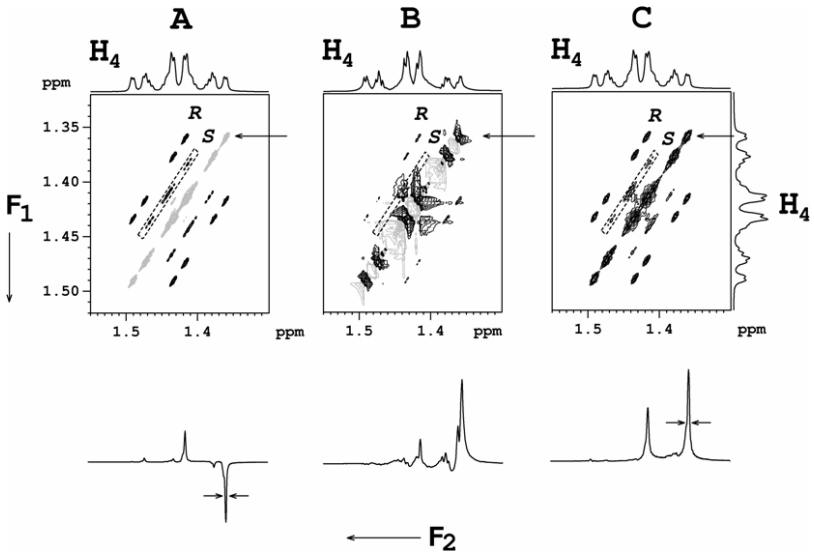

8.3.2. *Application of z-COSY for (R/S)-propylene carbonate, a six spin system*

For demonstrating the application of this methodology, the 2D methyl group selected BASE-z-COSY spectra of (R/S)-propylene carbonate has been reported. For clarity and to bring out the beneficial effect of BASE-z-COSY, has been compared with BASE-β-COSY spectrum recorded both in phase sensitive and magnitude modes under identical experimental conditions. The expanded methyl regions of all the spectra are given in Fig. 16. It is evident from the spectra that there is one to one correspondence among the spectra in all respects except for the phase properties of the 2D contours. The phase distortion of the diagonal peaks is more predominant in BASE-β-COSY spectrum recorded in phase sensitive mode compared to absolute mode. This is obvious from the F_2 cross sections represented by an arrow plotted below each spectrum. The unacceptable distorted phase and large line widths in BASE-β-COSY spectra are also distinctly evident from the cross sections. On the other hand, the BASE-z-COSY sequence provides cleaner spectrum with pure phase, lower line width giving enhanced resolution and sensitivity. The differences in their line widths provide more clarity. For example, the line widths of the particular cross section plotted below for BASE-z-COSY and magnitude mode BASE-β-COSY are 1.3 and 1.9 Hz respectively. It is clear that the peaks corresponding to *S* enantiomer, marked with tilted broken rectangle is completely masked in phase sensitive version of BASE-β-COSY spectrum and are visible in the magnitude mode spectrum but with relatively larger line width.

Contained in Fig. 17 the 2D BASE-z-COSY spectrum pertaining to protons H6 and H7 and its counter part of BASE-β-COSY recorded in magnitude mode. The advantage of pure phase and better clarity in the resolution is clearly visible from the expanded regions of a particular cross peak marked with broken rectangle. The peak separations of 2.4 and 1.0 Hz could be easily measured from the BASE-z-COSY spectrum. On the other hand in the BASE-β-COSY spectrum the multiplet pattern is poorly resolved for the peak with separation of 2.4 Hz and is significantly broadened for the peaks with coupling strength of 1.0 Hz, thereby restricting the measure of such a small coupling. This becomes clearer from the F_2 cross sections plotted below each of these expansions.

Figure 17: (A) and (C) The expanded cross peak multiplet patterns of BASE-z-COSY spectrum. B and D) The magnitude mode BASE-β-COSY spectra corresponding to protons H6 and H7 respectively. One of the cross peak multiplet pattern marked with broken rectangle designated by the arrows are plotted adjacent to each of the 2D data matrix. The cross section pertaining to top doublet pattern of the expanded part is plotted below each of them. The resolution achieved is evident from the well resolved contour in BASE-z-COSY and also their cross sections. Note: in H7 a doublet of small coupling is appearing as a broad hump in the BASE-β-COSY spectrum clearly bringing out the advantage of the BASE-z-COSY experiment.

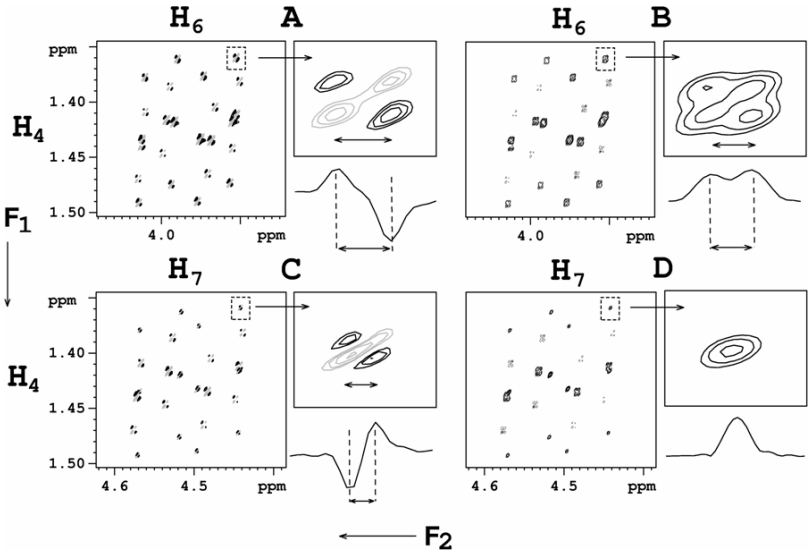

Another problem to be combated in phase sensitive COSY experiment is the presence of artifacts[58]. This is evident from the expansions of the spectra for proton H5 for both BASE-β-COSY and BASE-z-COSY given in Fig. 18. There are additional unacceptable artifacts in BASE-β-COSY spectrum, which are represented by a tilted broken line. The zero quantum filter, on the other hand, allows only the desired longitudinal magnetization and suppresses all other unwanted coherences in BASE-z-COSY spectrum.

Figure 18: The BASE-z-COSY and BASE-β-COSY spectra pertaining to proton H4 of (R/S)-propylene carbonate in the liquid crystal solvent PBLG, both recorded in phase sensitive modes. The presence of artifact in BASE-β-COSY spectrum is represented by a broken tilted line. Note: the absence of this artifact and the clean spectrum in BASE-z-COSY.

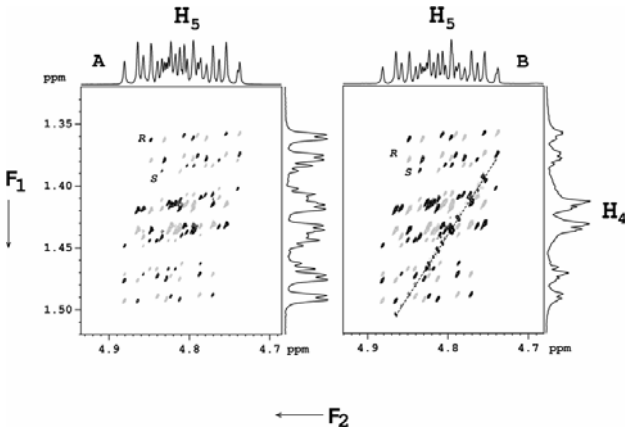

8.3.3. *z-COSY and reduced experimental time*

The major advantage of BASE-z-COY is in large saving of the experimental time. The minimum number of accumulations required for each t_1 increment is four for the phase sensitive BASE-β-COSY experiment. On the other hand in the BASE-z-COSY experiment we have used only two accumulations per t_1 increment. This resulted in the reduction of the instrument time by a factor of half. As a matter of comparison, experimental time requirement for the conventional z-COSY is 6–8 h, it is nearly 2 h for the aliased spectrum, and are 1.5 h and 45 min respectively for the phase sensitive version of BASE-β-COSY and BASE-z-COSY experiments with same number of t_1 increments required for the measurement of all the couplings. As far as deriving the spectral information is considered the analyses of the spectrum at individual chemical shift positions of different protons provides $({}^{n}T_{HH})^{R/S}$.

Figure 19: The 500 MHz phase sensitive z-COSY spectrum of (R/S)-Ibuprofen aligned in the liquid crystal solvent PBLG. The one dimensional ^{1}H spectrum and the chemical structure of the molecule with assignment to different protons, are given on the top. The size of 2D data matrix is 4096 × 4096. Spectral widths are 4455 and 4464 Hz in F_1 and F_2 dimensions. Number of accumulations for each t_1 increment is 2. The relaxation delay is 2.0 s. The data was zero filled to 4096 and 8192 points in F_1 an F_2 and processed with a 90° shifted sine bell window function. The digital resolution in both F_1 and F_2 dimensions are 1.1 Hz. Expansions of the regions A–C, marked with broken rectangle, are also given. The R and S enantiomers are marked for some of the peaks. The separations providing the couplings (in Hz) for Renantiomer are; $a = {}^2T_{H13H13} = 55.0$, $b = {}^3T_{H13H12} = 34.0$, $e = {}^2T_{H7H7} = 147.0$, $g = {}^3T_{H7H8} = 37.0$. For S enantiomer the separation providing the couplings (in Hz) are; $c = {}^2T_{H13H13} = 82.5$, $d = {}^3T_{H13H12} = 46.5$, $f = {}^2T_{H7H7} = 178.0$, $g = {}^3T_{H7H8} = 37.0$. Note: the value of g is same for both the enatiomers and hence the separation is denoted by the same alphabet.

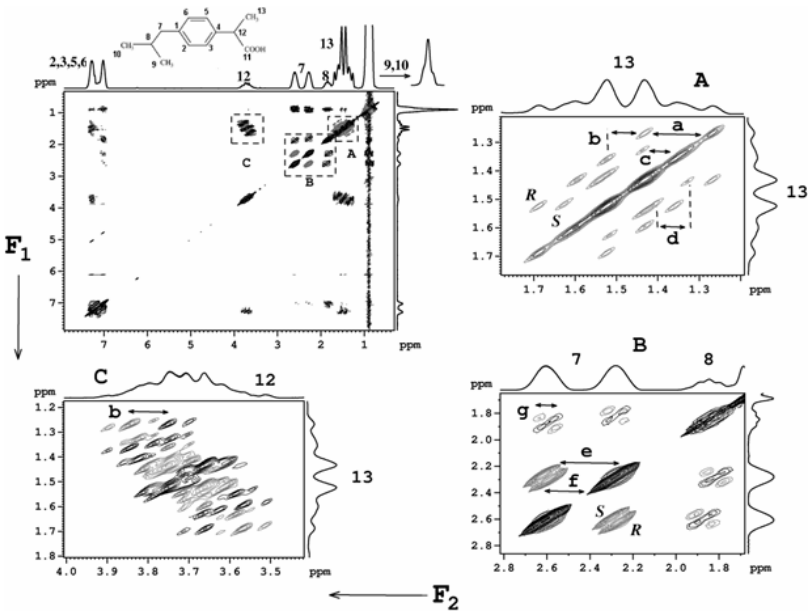

8.3.4. *Application of z-COSY to bigger chiral molecules*

The z-COSY/BASE-z-COSY can in principle be applied for getting higher resolution in bigger chiral molecules. To demonstrate this application the pure phase z-COSY spectrum of (R/S)-Ibuprofen, which has 17 protons and an OH group uncoupled to other protons has been reported. This molecule has already been partially analysed in PBLG liquid crystal[59]. Its z-COSY spectrum and the expansions of different regions of the spectrum for assigned protons are given in Fig. 19. Though the order parameter is very small it is apparent from the magnified intensity scale of the spectrum, all the protons are coupled among themselves. Hence though the spin system is weakly coupled, and many long distance couplings could be small, the numerical iterative analysis pertains to a 17 coupled spin system, which is computationally intensive and has not been reported. The visualization of enantiomers and extract some of the couplings in the racemic mixture is very tedious. Studies imply that the utilization of ^{1}H NMR for accurate chiral analyses for bigger molecules of real pharmaceutical interest appear to be very promising but still demands methodological developments for complete analyses of the spectra.

8.3.5. *z-COSY and the quantification of enantiomeric excess*

Apart from the measurement of couplings the z-COSY spectrum can also be applied for quantitative measurements[49]. An ideal situation for a measurement of couplings and enantiomeric excess (ee) would be the significantly larger values of active coupling compared to the line width, where the antiphase components do not cancel each other. On the other hand for active couplings of comparable or smaller than the linewidth the antiphase components will cancel each other partially and integration is not precise.

This concept has been utilized for the measure of ee in a scalemic mixture of 21% excess of R enantiomer. For such a measurement, well resolved

Figure 20: (A and (B) The 500 MHz BASE-z-COSY spectrum of a scalemic mixture (21% excess of R enantiomer) of (R/S)-propylene carbonate oriented in PBLG for protons H6 and H7. The R and S enantiomers are marked. The contours chosen for the measurement of areas to determine enantiomeric excess are denoted by broken rectangles. The numbers 1 and 2 are pairs of contours of the particular multiplet component belonging to each enantiomer. (C) and (D) One of the contour pairs, 1, is expanded below each of them.

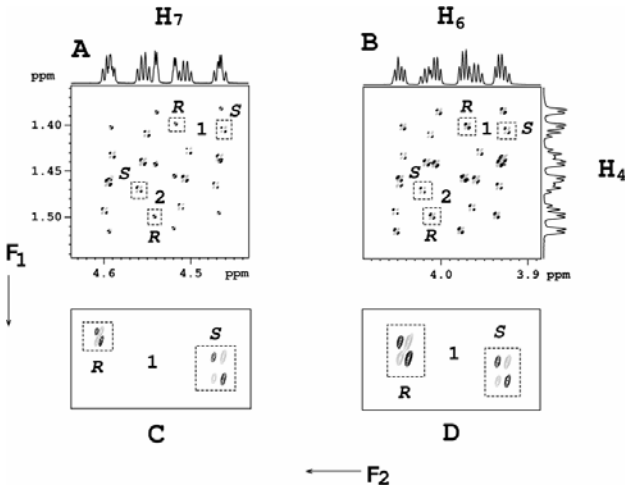

contours of the z-COSY spectrum, marked 1 and 2 of identical multiplet component of protons H6 and H7 of (R/S)-propylene carbonate, reported in Fig. 20 have been chosen. The contour marked 1 is further expanded below each 2D matrix. For proton H6 (Fig. 20B) the areas of the contours 1 and 2 provided the excess ratio of 22% each. On the other hand the similar measurement using proton H7 (Fig. 20A) provided large errors for both the contours. This is due to the fact that in H6 the coupling strengths and the peak separations for both R and S enantiomers were nearly same (2.1 Hz). For proton H7 the coupling strength of R form is 1.0 Hz and that of S form is 2.4 Hz. The large differential values lead to measurement errors, because of the partial cancellation by the anti phase peaks from the R enantiomer giving rise to fictitiously erroneous contour areas as discussed above.

It is also well known that for quantitative measurement of intensities or the areas of peaks, one is required to wait for five times the longitudinal relaxation time (T_1), which is of the order of few seconds. In the reported study the T_1 values of the protons have been measured using the standard inversion recovery method. The values ranged from 2.2 to 2.6 s for different peaks. Thus the relaxation delay between successive accumulations of free induction decay should be around 10–11 seconds. This implies in the normal correlated experiment such as, COSY, z-COSY, etc. the total experimental time would be around 14 h, whereas for BASE-z-COSY it was nearly 2 h.

9. Triple quantum two dimensional methodology

The DQ-SERF sequence developed for eanantiomeric discrimination employed selective excitation of DQ coherence of coupled methyl protons for better eanantiomeric discrimination and provided well resolved and simplified spectrum in the DQ dimension. The coupling among methyl protons could be extracted from the DQ dimension. However, the enantiopure spectrum obtainable from the SQ dimension is very complex due to the presence of too many short and long distance couplings experienced by each proton. Thus the determination of all the remote couplings from the cross section taken along any peak in the DQ dimension is difficult. However, the determination of all the coupling parameters is crucial when one is interested in the determination of the molecular order. Therefore, there are several problems remain to be combated, viz., the simplification of spectra in each cross section, obtaining high resolution, the determination of the relative signs and magnitudes of all the proton-proton couplings. One of the ways of combating this is the spin state selective detection to simplify the spectra in each cross section by separating active and passive couplings into different sub spectra containing fewer transitions as in two dimensional correlation experiments discussed in the previous sections. This could be achieved by editing the SQ transitions using the spin states of the passive spins. When the dipolar coupled methyl protons are concerned 3Q-SQ correlation is a feasible option. This is of particular interest as this can be very informative in contrast to isotropic studies where the couplings among methyl protons are not reflected in spectra. In addition, the spin state selective detection is also possible for non-equivalent protons.

The spin state selective detection has been developed by spin selective correlation of triple quantum (3Q)-SQ coherence[60] of the methyl protons and the retention of the entire passive homonuclear couplings in 3Q dimension by the application of a non-selective refocusing pulse. The method also overcomes the problem of field inhomogeneity in addition to providing very high resolution. With 3Q excitation of the methyl protons, the 3Q dimension retains the long distance small couplings (passive couplings) enhanced by a factor of three, whereas the SQ dimension retains only the short distance couplings (active couplings). The differential scaling of dipolar couplings in the R

Figure 21: (A) The pulse sequence used for the selective excitation of 3Q coherence of methyl group in molecules (R/S)-2-chloropropanoic acid and (R/S)-3-butyn-2-ol. $\Phi_1 = X$, $\Phi_2 = Y$, $\Phi_3 = Y$, receiver phase (Φ_R) is x and the selection of desired coherence pathway is achieved by the gradients; B) The pulse sequence used for the selective excitation of 3Q coherence of methyl group for the molecules (R/S)-propylene carbonate and (R/S)-propylene oxide. Triple Quantum EXORCYCLE phase cycling is used for the non-selective 180° pulse in the middle of 3Q dimension. This pulse sequence serves as a spin state selective 3Q resolved experiment.

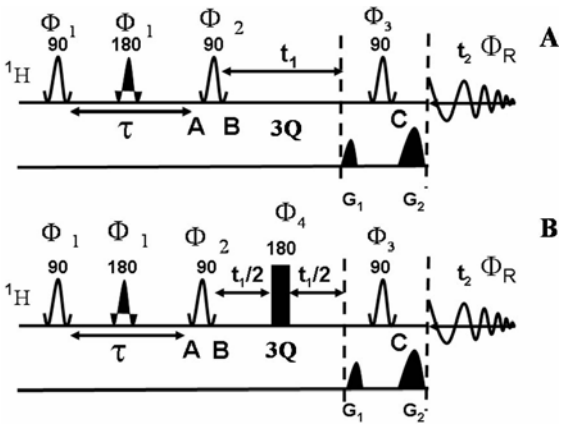

and *S* enantiomers enable discrimination and also provide spectral simplification. As far as the methyl groups are concerned, due to magnetic equivalence, the resolution in 3Q spectrum is three times that of SQ spectrum and hence unambiguous chiral visualization is possible. The complex multiplet pattern gets simplified, by the separation of active and passive couplings in different dimensions, for each enantiomer. Another novelty of this method is that all the D_{HH} participate in enantio discrimination unlike only one D_{HH} among methyl protons in DQSERF and SERF experiments. The pulse sequences employed for 3Q-SQ methodologies are given in Fig. 21. The methodology is discussed in detail below.

9.1. *Spin state selective coherence transfer and enantiomeric discrimination*

For spin state selective coherence transfer, two points are of vital importance; (a) couplings to a passive spin(s) should be retained in both the 3Q and SQ dimensions and (b) the 3Q-SQ conversion is carried out with spin selective pulse without disturbing the states of the passive spin(s). In such an experiment the $|\alpha\rangle$ domain of the 3Q coherence is correlated to its corresponding SQ coherences of $|\alpha\rangle$ domain only and there is no coherence transfer to SQ coherences of $|\beta\rangle$ domain. The identical analogy holds good for $|\beta\rangle$ domain 3Q coherence also. This is a vital difference compared to conventional non-selective 3Q-SQ correlation experiments.

The important features of this methodology in the context of enantiomeric discrimination are; (i) A complex multiplet pattern which is difficult to analyze in the one dimensional proton spectrum is simplified by separating into individual sub spectra in different cross sections depending on the passive spin states. Consequence of this is the separation of active and passive couplings leading to dramatically enhanced resolution in both SQ and 3Q dimensions, (ii) active couplings are present in each SQ cross section corresponding to each passive spin state in 3Q dimension, (iii) the separated sub spectra in different cross sections are displaced along SQ dimension. The magnitudes of these displacements provide the passive couplings, and (iv) the tilts of the displacement vectors provide relative signs of the couplings.

9.2. *Spin selective 3Q-SQ spectra of A_3 and A_3 MX spin systems*

The selectively A_3 spins excited 3Q-SQ coherence for the (R/S)-2-chloropropanoic acid and (R/S)-3-butyn-2-ol that pertains to A_3X and A_3MX spin systems are given in Fig. 22. The analysis of the spectra of these molecules is pretty straightforward.

When all the methyl protons are flipped in (R/S)-2-chloropropanoic acid, the 3Q dimension pertains to A part of an AX spin system. The A part of AX spin system is detected in the 3Q dimension, which is a doublet. This doublet separation is $3(^3T_{HH}) = 3(2x^3D_{HH} + {}^3J_{HH})$ rather than $^3T_{HH}$ between adjacent SQ transitions in a SQ spectrum and plays a prominent role in enhanced separation of enantiomer peaks. The triple quantum states of the A_3 protons are $|\alpha\alpha\alpha\rangle$ and $|\beta\beta\beta\rangle$. There are two 3Q transitions for each enantiomer which are, $|\alpha_A\alpha_A\alpha_A(\alpha_X)\rangle \rightarrow |\beta_A\beta_A\beta_A(\alpha_X)\rangle$ and $|\alpha_A\alpha_A\alpha_A(\beta_X)\rangle \rightarrow |\beta_A\beta_A\beta_A(\beta_X)\rangle$, corresponding to $|\alpha\rangle$ and $|\beta\rangle$ spin states of the passive spin X. Thus the two cross sections corresponds to passive proton spin states $|\alpha\rangle$ and $|\beta\rangle$. Thus the spin state selective detection of A_3 SQ transitions is achieved. For the transition within each sub spectrum, the spin state of X remains undisturbed in both t_1 and t_2 dimensions. The coupling to methine proton is removed in each cross section resulting in half the number of transitions compared to one dimensional spectrum and hence high resolution in the SQ dimension. This allows the precise measurement of $^2T_{HH}$. Therefore, in a single experiment not only one can determine both $^2T_{HH}$ and $^3T_{HH}$ but also separate them which were not possible from any earlier reported experiments in the literature. This reduced the spectral complexity arising out of too many couplings leading to unresolved transitions in a single dimension and aids in the simplification of enantiomer spectra.

Figure 22: The 500 MHz ^{1}H 2D 3Q-SQ correlation spectrum of selectively excited methyl protons (using pulse sequence given in Fig. 21A) in; (A) (R/S)-2-chloropropanoic acid, α_R, β_R and α_S, β_S are the two spin states of the passive proton for the enantiomers R and S respectively. The expansion of the two contours of the 2D matrix shown clearly identifies the two peaks of the enantiomers. The separations depicted in alphabets provide coupling information. For R enantiomer: $a = {}^2T_{H4H4}$ and $b = {}^3T_{H4H5}$. For S enantiomer; $c = {}^2T_{H4H4}$, $d = {}^3T_{H4H5}$; (B) (R/S)-3-butyn-2-ol. The $R_{|\alpha\alpha\rangle}$, $R_{|\alpha\beta\rangle}$, $R_{|\beta\alpha\rangle}$ and $R_{|\beta\beta\rangle}$ and $S_{|\alpha\alpha\rangle}$, $S_{|\beta\alpha\rangle}$, $S_{|\alpha\beta\rangle}$ and $S_{|\beta\beta\rangle}$ are the spin states of the passive protons for the enantiomers R and S respectively. The separations depicted in alphabets provide coupling information. For R enantiomer: $a = {}^2T_{H7H7}$, $b = {}^3T_{H6H7}$ and $c = {}^5T_{H5H7}$. For S enantiomer; $d = {}^2T_{H7H7}$, $e = {}^3T_{H6H7}$ and $f = {}^5T_{H5H7}$. Notice the quality of discrimination achieved in the 3Q dimension.

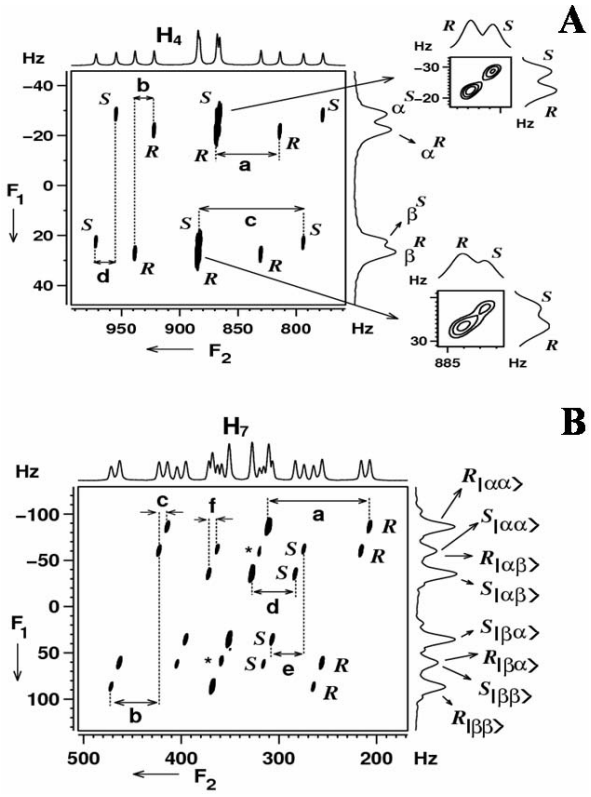

In addition to enhanced scaling of dipolar couplings, there is also an advantage due to the scaling of the chemical shift anisotropy for chiral discrimination. The difference in anisotropic chemical shifts between the R and S enantiomers in the SQ dimension is 4.6 Hz. Though it is possible to visualize in the one dimensional spectrum, it is better visualized in 3Q dimension. Due to magnetic equivalence of methyl protons, this value is also enhanced three times in the 3Q dimension which can be viewed after discrimination by comparing the centre of the two separated R and S spectra. The separations, marked a and b provide, $^2T_{H4H4}$ and $^3T_{H4H5}$ respectively for the Renantiomer. The separations c and d provide similar information for the S enantiomer.

In (R/S)-3-butyn-2-ol, when all the three methyl protons are flipped the spin system in the 3Q dimension is of the type AMX, where A is the super spin with three methyl protons, M is the methine proton and X is the acetylenic proton respectively. The A part of this AMX spin system is detected in the 3Q dimension. Corresponding to four spin states $|\alpha\alpha\rangle$, $|\alpha\beta\rangle$, $|\beta\alpha\rangle$ and $|\beta\beta\rangle$ of the passive spins M and X, there are four allowed 3Q transitions for spin A arising from each enantiomer, unlike 12 transitions in a SQ spectrum. Thus there is enhanced resolution in the 3Q dimension. The cross sections taken along the SQ dimension for each spin state of an enantiomer provides only the active coupling between the methyl protons, which is a triplet. There are four such triplets pertaining to four A_3 sub spectra in different cross sections. Thus high resolution is achieved in SQ dimension also. Four such cross sections with identical active coupling unambiguously differentiate the peaks arising from each enantiomer. From the 3Q dimension the passive coupling information, $^3T_{HH}$ and $^5T_{HH}$, could be determined directly.

9.3. *Application of 3Q-SQ correlation for bigger spin systems*

As discussed earlier methyl region of one dimensional spectra of (R/S)-propylene carbonate and (R/S)-propylene oxide consist of 24 transitions for each enantiomer. The twenty four transitions observed for methyl groups can be construed as eight A_3 sub spectra corresponding to eight spin states of M, N and X together. The complexity is obvious from their one dimensional spectra (Fig. 1), where one can see that the methyl protons are resonating in a narrow spectral width of 90 Hz in (R/S)-propylene carbonate and 40 Hz in (R/S)-propylene oxide. The broad and featureless spectrum due to too many long distance couplings makes it impossible to recognize any fine structure. Achieving both high resolution in 3Q dimension and spin state selective detection in spite of very small unresolved couplings from the two inequivalent methylene protons is a challenge. This 3Q dimension gives a broad signal arising due to the contributions from the field inhomogeneity. The inhomogeneity contribution increases linearly with the detection of the higher quantum order. Therefore, the 3Q order has three times the enhanced signal broadening. One method to remove this field inhomogeneity contribution is to apply a non-selective 180° pulse in the middle of the t_1 dimension which refocuses the chemical shifts and retains all the passive couplings for the spin state selection. The experiments on (R/S)-propylene oxide performed using the pulse sequence given in Fig. 21B and the corresponding spectra are given in Fig. 23. The dramatic improvement in the resolution in 3Q dimension is clearly evident.

Figure 23: A) The 2D 3Q-SQ correlation spectrum of selectively excited methyl protons in (R/S)-propylene carbonate using pulse sequence given in Fig. 21B. The separations depicted in alphabets provide coupling information. They are for S enantiomer: $a = {}^2T_{H4H4}$, $b = {}^3T_{H4H5}$, $c = {}^4T_{H4H6}$ and $d = {}^4T_{H4H7}$. For R enantiomer; $e = {}^2T_{H4H4}$, $f = {}^3T_{H4H5}$, $g = {}^4T_{H4H6}$ and $h = {}^4T_{H4H7}$. Two types of ${}^4T_{HH}$ (between 4 and 6, between 4 and 7) are equal for the S enantiomer. (B) 2D 3Q-SQ correlation spectrum of selectively excited methyl protons in (R/S)-propylene oxide. The separations represented by different alphabets provide coupling information. The values in Hz are for S enantiomer: $a = {}^2T_{H7H7}$, $b = {}^3T_{H4H5}$ and $c = {}^4T_{H4H6}$. The separation ${}^4T_{H4H7}$ is not detectable due to its small strength. For R enantiomer: $d = {}^2T_{H7H7}$, $e = {}^3T_{H4H5}$, $f = {}^4T_{H4H6}$ and $g = {}^4T_{H4H7}$.

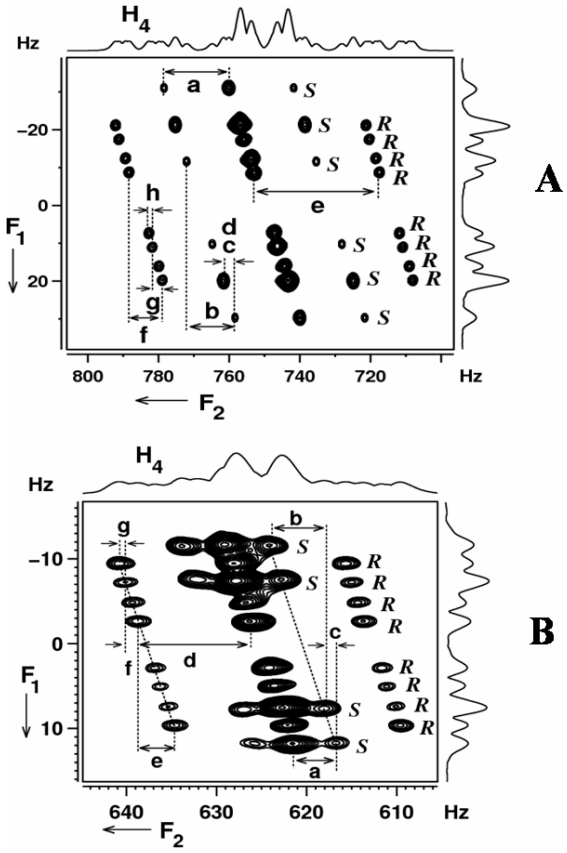

9.4. *Interpretation of 3Q-SQ spectra of A_3MPX spin system*

As far as the analyses of the 3Q-SQ spectrum, reported in Fig. 23, is concerned, the spin systems are of the type AMPX in the 3Q dimension, where A is the super spin with 3 methyl protons and passive spins M, P and X are protons. The ${}^2T_{HH}$ in A_3 are the active couplings while one ${}^3T_{HH}$ and two ${}^4T_{HH}$ constitute the passive couplings. The 3Q dimension must result in eight transitions for each enantiomer pertaining to eight spin states of M, P and X together.

The eight well resolved transitions were detected for R enantiomer. However, for the S enantiomer only four transitions are observed due to negligible strength of one of the remote couplings, which is clearly evident from the spectrum. This is due to the fact that the residual dipolar coupling D_{H4H6} is opposite in sign to that of through bond coupling J_{H4H6} and hence $T_{H4H6} = 0$. The separations marked in Fig. 23 provide the spectral parameters. Another 3Q-SQ correlation experiments with 5, 6 and 7 protons as active spins and methyl protons are passive spins have also been carried out for both the molecules. Both 3Q-SQ experiments together provided all the couplings of the molecule.

9.5. *The advantages of triple quantum-single quantum correlation experiments*

The pulse sequences discussed in the previous section have numerous advantages in the context of chiral discrimination and the analyses of broad and unresolved ^{1}H spectra. They can be listed as;

1. The dramatically enhanced resolution has been obtained in the otherwise broad and featureless spectra and the peaks that were separated by as low as separation 0.65 Hz could be measured.
2. In spin selective 3Q-SQ correlation experiments, the values of ${}^nT_{HH}$ $(n = 2, 3, 4, 5)$ being different for both the enantiomers, there was an unambiguous chiral discrimination in both the dimensions.
3. The active and passive couplings are separated from each other in a single experiment and both are utilized for discrimination. Active couplings are present in each cross section while passive couplings are responsible for the displacement of the sub spectra.
4. Using two selectively detected 3Q-SQ experiments the complete analyses of the overlapped spectra of both the enantiomers in six spin systems, viz., (R/S)-propylene carbonate and (R/S)-propylene oxide have been carried out.
5. In the methyl group excited experiments the resolution in the 3Q dimension is $3({}^nT_{HH})$ and one in the SQ dimension results in a net total chiral dispersion of 3.3 times in the tilted direction as far as the measurement of the resonance frequencies between the chiral molecules is concerned. The difference between consecutive R and S peaks $\{T^R(={}^nT_{HH}) - T^S(={}^nT_{HH})\}$ becomes $3 \times \{T^R(={}^nT_{HH}) - T^S(={}^nT_{HH})\}$ in 3Q dimension which contributed to better chiral discrimination. In the earlier SERF experiments the consecutive R and S peak separation was only $\{T^R(={}^nT_{HH}) - T^S(={}^nT_{HH})\}$.

Figure 24: The 500 MHz proton 4Q-SQ correlated 2D spectrum of (R/S)-2-chloropropanoic acid aligned in the chiral liquid crystal PBLG. The t_1 and t_2 dimensions correspond respectively to 4Q and SQ coherences. One dimensional spectrum given below the 2D spectrum is the cross section taken along SQ dimension at the position of S enantiomer in the 4Q dimension. Due to large width of the contours along the F_1 axis, the less intense peaks from R enantiomer are also seen in the cross section.

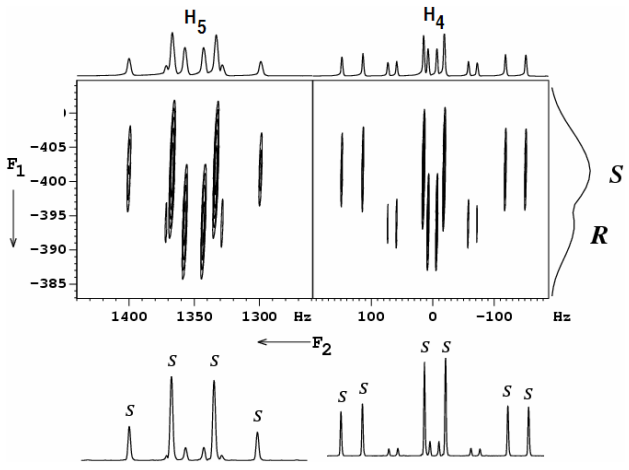

6. The difference in $\Delta\sigma_i$ between the two enantiomers is also enhanced three times in 3Q dimension as is seen from the difference in the mean frequencies of the doublets of the two enantiomers in (R/S)-2-Chloropropanoic acid (Fig. 22A).
7. The comparison of the tilt directions of the multiplets in different cross sections for different chemical shift positions provides the relative signs of the couplings.
8. In favourable cases, the parameters derived from the 2D spectra can be used for the iterative analysis to derive all other spectral parameters. This simplifies the analyses to a large extent.

10. Chiral discrimination in the absence of the dipolar or quadrupolar field

In all the single quantum, double quantum and triple quantum correlation experiments discussed in the previous sections, the presence of dipolar couplings among protons is utilized for the visualization of enantiomers. A method has also been proposed for chiral discrimination and to obtain enantiopure spectra from the racemic mixture in the absence of dipolar fields[61]. The chemical shift anisotropy of protons $(\Delta\sigma_H)$ has been employed as an exclusive parameter for such a purpose. The magnitudes of $\Delta\sigma_H$ are inherently smaller and are within a few ppm even in thermotropic liquid crystals where the orientational parameters are several orders of magnitudes larger than in weakly ordered chiral liquid crystal. In the weakly aligned chiral liquid crystals, in general, it is imperative that $\Delta\sigma_H$ is immeasurably smaller resulting in an indistinguishable overlap of the transitions from both the enantiomers. If on the other hand the sum of the chemical shift anisotropies of all the protons of one enantiomer is different from that of the other, and is of measurable magnitude, the enantiodiscrimination can still be achieved. This concept has been exploited in the reported work[61].

The pulse sequence utilizes the non-selective excitation of homonuclear highest quantum of all the coupled protons resulting in their simultaneous flipping. This is a situation when all the protons of the molecule are simultaneously flipped. Neither the scalar nor the dipolar couplings influence the spectrum and the magnetization in the multiple quantum (MQ) dimension will evolve at the sum of their anisotropic chemical shift values providing a singlet for each enantiomer. In the higher quantum dimension the cumulative additive value of anisotropic chemical shifts of each enantiomer provides a sizeable differential value between the enantiomers enabling the complete unraveling. Since the basic requirement is the coupling among all the protons, this methodology is applicable to small and medium sized molecules. The selective detection of the particular order of the quantum is achieved by employing the gradients.

An application of this methodology has been demonstrated for (R/S)-2-chloropropanoic acid whose two dimensional MQ-SQ correlated spectra are given in Fig. 24. The differences in the individual values of $\Delta\sigma_i$ of methyl protons and the methine proton between the enantiomers are negligibly small. As the cumulative additive value of $\Delta\sigma_i$ will evolve in the highest quantum, the fourth quantum coherence was allowed to evolve in the indirect dimension. The higher quantum dimension thus will have two identifiable transitions, each of which corresponds to one of the enantiomers. The cross sections taken along the SQ dimension at the resonating positions of each peak in the 4Q dimension pertain to the one dimensional spectrum of an enantio pure sample. The literature knowledge of assignment for R and S enantiomers reported for one dimensional experiment aided the assignment of peaks to R and S enantiomers in the 4Q dimension. The cross section taken along SQ dimension for S enantiomer, plotted below the 2D spectrum (Fig. 24), is an enantiopure spectrum. Thus even in the absence of dipolar fields the chemical shift anisotropy could be used as an exclusive parameter for unambiguous discrimination and complete unraveling of the spectra for each enantiomer.

Figure 25: (A) The pulse sequence employed for CH-SERF experiment. The behaviour of the magnetization during different stages of pulse sequences are discussed in the text. Rectangular pulses are hard pulses. All the remaining pulses are spin selective. The phases of the pulses are; $\phi_1 = x,\ \phi_2 = x\ x - x\ -x,\ \phi_3 = y;\ \phi_4 = 4(x)\ 4(-x),\ \phi_5 = x\ -x,$ $\phi_6 = \phi_7 = 8(x)\ 8(-x)$ and $\phi_R = 2(x\ -x)\ 4(-x\ x)\ 2(x\ -x)$. (B) The pulse sequence used for CH-DQSERF experiment. The phases of the pulses are $\phi_1 = x,\ \phi_2 = 4(x)\ 4(-x),\ \phi_3 = y;\ \phi_4 = 8(x)\ 8(-x),\ \phi_5 = 4(x\ -x),$ $\phi_6 = \phi_7 = (8)x,\ \phi_8 = 2(x)\ 2(y)\ 2(-x)\ 2(-y),\ \phi_R = 4(x\ -x)\ 4(-x\ x)$. The delay τ_1 responsible for the polarization transfer depends on the factor $1/(4(^1T_{AX}))$ and was adjusted for each molecule independently, the gradient ratio used was G2:G3 = 1:2.

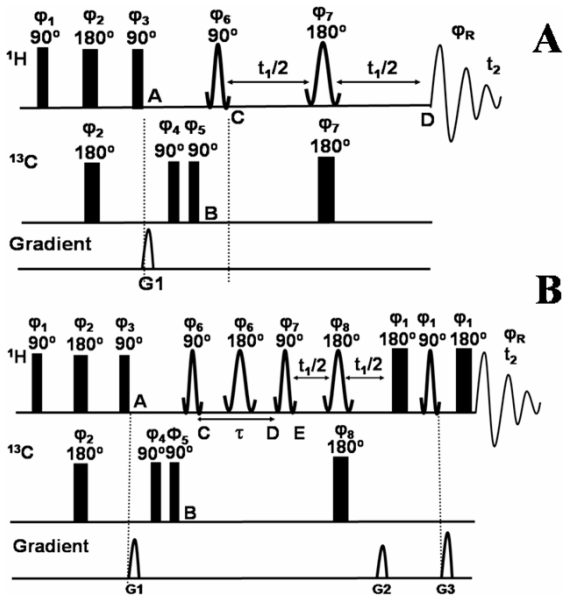

11. Use of natural abundant ^{13}C as a spy nucleus

With more number of passive couplings participating in the higher quantum dimension, there will be improved discrimination of the *R* and *S* enantiomers. In other words discrimination should be benefited from the difference of as many parameters as possible. In such situations one can derive the advantage of the comparatively larger value of heteronuclear coupling. However, as discussed in the earlier, with every addition of an interacting spin, the number possible single quantum transitions increase nearly by a factor of four. Therefore the inclusion of ^{13}C in its natural abundance as a participating spin poses several challenges, such as, sensitivity enhancement, identification of ^{13}C satellite transitions for each enantiomer from the broad and featureless ^{1}H spectrum and simplification of the spectra for determination of both homo and heteronuclear couplings. Several methods have been developed to combat these problems and are discussed in the following sections.

11.1. *Single and double quantum resolved techniques*

The resolved techniques using natural abundant ^{13}C spin are the development of reported SERF[28] and double quantum selective refocusing (DQ-SERF) experiments[31] utilizing INEPT (Insensitive Nuclei Enhanced by Polarization Transfer)[62] for enhancing the signal intensity. The use of INEPT sequence for the visualization of enantiomers in heteronuclear correlation experiments is well known[63,64]. The present techniques apply INEPT for two dimensional resolved experiments. The pulse sequences are the blend of INEPT with two dimensional spin selective single quantum and double quantum coherences and are designated as CH-SERF and CH-DQSERF respectively. The designed experiments aid in chiral discrimination and also simultaneous determination of homonuclear (D_{HH}) and heteronuclear (D_{CH}) couplings. The techniques are demonstrated on different chiral molecules[65]. The CH-SERF and CH-DQSERF pulse sequences are reported in Fig. 25.

11.1.1. *Evolution of magnetization in the pulse sequences*

The polarization operator formalism[27] is employed for understanding the spin dynamics and the appearance of the two dimensional spectra in CH-SERF and CH-DQSERF pulse sequences. For discussion a weakly dipolar coupled spin system of the type A_3MX (where A and M are proton spins and X is a carbon spin) is chosen. Spectrum of such a spin system is influenced by two types of homonuclear couplings, $^2T_{AA}$ and $^3T_{AM}$ and one heteronuclear coupling $^1T_{AX}$, The parameter $^2T_{MX}$is not detected since the selective pulses are applied only on A_3 spins.

The CH-SERF pulse sequence (Fig. 25A) starts with a non-selective INEPT from ^{1}H to ^{13}C spin resulting in a term $I_z^A S_y^X$ (where I is proton and S is carbon) after the first hard $(\pi/2)_x$ pulse on ^{13}C. The gradient employed after the second $(\pi/2)_y$ pulse on I spin suppresses the proton magnetization attached to ^{12}C. The magnetization transfer pathway during the second half (during A to B) of the pulse sequence can then be described as

$$I_z^A S_y^X \xrightarrow{(\Pi/2)_x^X} I_z^A S_z^X \xrightarrow{(\Pi/2)_x^A} I_y^A S_z^X \qquad (21)$$

The INEPT transfer enables the spin state selection by ^{13}C nucleus. This followed by the selective excitation of A spin single quantum coherence leading to $I_y^A S_z$ term at the time point B. From the stage B to C, the magnetization evolves under $^2T_{AA}$ and $^1T_{AX}$ couplings due to selective 180° pulse on A_3 and a hard 180° pulse on X in

Figure 26: The 500 MHz CH-SERF spectrum of (R/S)-2-chloropropanoic acid oriented in the liquid crystal PBLG. The $|^{13}C_\alpha\rangle$ and $|^{13}C_\beta\rangle$ regions marked in the F_1 dimension pertains to two spin states of ^{13}C. The peaks for R and S enantiomers are labeled. The expansion of a small region of the spectrum given in the inset depicts the resolution of closely resonating transitions. The magnitudes of the couplings (in Hz) are; $a = (^3T_{HH})^R = 19.3$, $b = (^1T_{CH})^R = 113.0$, $c = (^2T_{HH})^R = 37.2$ and $d = (^3T_{HH})^S = 6.2$, $e = (^1T_{CH})^S = 142.0$ and $f = (^2T_{HH})^S = 22.3$.

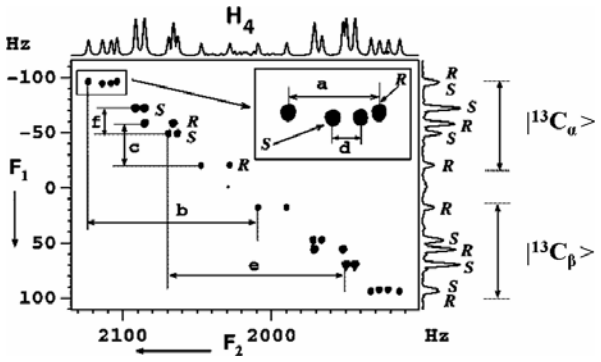

the middle of t_1 dimension. Thus the polarization operator (i.e, $I_y^A E^A E^A S_z^X$) that evolves during the t_1 period is

$$\frac{1}{8}(I_+^A)[(I_\alpha^A + I_\beta^A)][(I_\alpha^A + I_\beta^A)](S_\alpha^X - S_\beta^X) \qquad (22)$$

The resulting spectrum in the t_1 dimension will be doublet of a triplet arising from the dipolar couplings between A_3 spins and the states $|\alpha\rangle$ and $|\beta\rangle$ of ^{13}C spin respectively. The absence of mixing pulse leaves the spin states of both ^1H and ^{13}C unperturbed in both t_1 and t_2 dimensions. During the t_1 period, the coupling $^3T_{AM}$ is refocused and is retained during the t_2 period. The polarization operator during the t_2 period will then be

$$\frac{1}{16}(I_+^A)[(I_\alpha^A + I_\beta^A)][(I_\alpha^A + I_\beta^A)](I_\alpha^M + I_\beta^M)(S_\alpha^X - S_\beta^X) \qquad (23)$$

The spectrum is, therefore, a doublet of doublet of a triplet in the t_2 dimension. These six transitions appear as doublets along t_2 dimension corresponding to six states of A_3X spins.

The discussion for CH-DQSERF pulse sequence (Fig. 25B) is identical to that of sequence shown in Fig. 26A up to the point B. During the pathway from B to D, the magnetization evolves under $^2T_{AA}$ coupling since the selective 180° pulse decouples A_3 from both M and X spins and the second selective 90° pulse between time points C and D creates double quantum $I_y^A I_y^A I_z^A S_z^X$ coherence at the point D. The polarization operator during the t_1 period is

$$\frac{1}{4}(I_+^A I_+^A - I_+^A I_-^A - I_-^A I_+^A + I_-^A I_-^A)(I_\alpha^A + I_\beta^A)(S_\alpha^X - S_\beta^X) \qquad (24)$$

The hard 180° pulse on ^{13}C and the selective 180° pulse on A_3 in the middle of t_1 dimension ensure the evolution of double quantum $(I_+^A I_+^A)(I_\alpha^A + I_\beta^A)(S_\alpha^X - S_\beta^X)$ term under $^2T_{AA}$ and $^1T_{CH}$ couplings. The frequency gets modulated in the t_1 dimension as

$$\begin{aligned} &\exp[+i(2\Omega_A - \pi k_1 - \pi k_2)t_1] \\ &\quad + \exp[+i(2\Omega_A + \pi k_1 - \pi k_2)t_1] \\ &\quad - \exp[+i(2\Omega_A - \pi k_1 + \pi k_2)t_1] \\ &\quad - \exp[+i(2\Omega_A + \pi k_1 + \pi k_2)t_1] \end{aligned} \qquad (25)$$

where $k_1 = {}^2T_{AA} + {}^2T_{AA}$ and $k_2 = {}^1T_{AX} + {}^1T_{AX}$

The spectrum in t_1 dimension will then be a doublet of a doublet, which is in phase with respect to sum of passive homonuclear couplings (k_1) and antiphase with respect to the sum of passive heteronuclear couplings (k_2). The last selective $(\pi/2)_X$ pulse on A_3 spins converts double quantum term to the single quantum term. Since $^3T_{AM}$ is present in t_2 dimension the polarization operator terms after spin selective DQ-SQ conversion corresponding to $|\alpha\rangle$ spin state of passive spin A are;

$$\begin{aligned} \frac{1}{4i}(I_+^A I_+^A)(I_\alpha^A)(S_\alpha^X - S_\beta^X) \rightarrow\ & \frac{1}{8}(I_-^A)[i(I_\alpha^A - I_\beta^A)] \\ & (I_\alpha^A + I_\beta^A)(I_\alpha^M + I_\beta^M) \\ & (S_\alpha^X - S_\beta^X) \end{aligned} \qquad (26)$$

[t_1 dimension] [t_2 dimension]

Thus, the spectrum in the t_2 dimension will be doublet of doublet of a triplet.

11.1.2. *Analyses of CH-SERF spectra of (R/S)-2-chloropropanoic acid*

The protons and carbon of the methyl group of this molecule form a weakly coupled spin system of the type A_3MX where A_3 corresponds to methyl protons and M is the methine proton and X is the ^{13}C coupled to methyl protons. Since the pulse scheme involves a non-selective INEPT transfer of magnetization from ^1H to ^{13}C and then back transfer to proton, the ^{13}C edited proton magnetization is subsequently employed for selective refocusing. In the middle of the t_1 dimension, the simultaneous application of a selective refocusing π pulse on the methyl protons and a non-selective π pulse on ^{13}C retains $^1T_{CH}$ and $^2T_{HH}$ couplings of the methyl group and refocuses all the remote $^3T_{HH}$ couplings. This enhances the resolution in the t_1 dimension.

The selective methyl protons excited 2D CH-SERF spectrum of this molecule is reported in

Figure 27: A) The ^{12}C attached selective methyl group excited 2D SERF spectrum of (R/S)-2-chloropropanoic acid aligned in PBLG liquid crystal with the F_1 and F_2 projections. The peaks for R and S enantiomers are labeled. $*$ Marks indicate the overlap of two transitions from R and S. The magnitudes of the couplings (in Hz) are; $a = ({}^3T_{HH})^R = 19.3$, $b = 2({}^2T_{HH})^R = 74.4$, $c = ({}^3T_{HH})^S = 6.2$ and $d = 2({}^2T_{HH})^S = 44.6$, and (B) The Expanded $|{}^{13}C_\alpha\rangle$ region of Fig. 26A given for comparison.

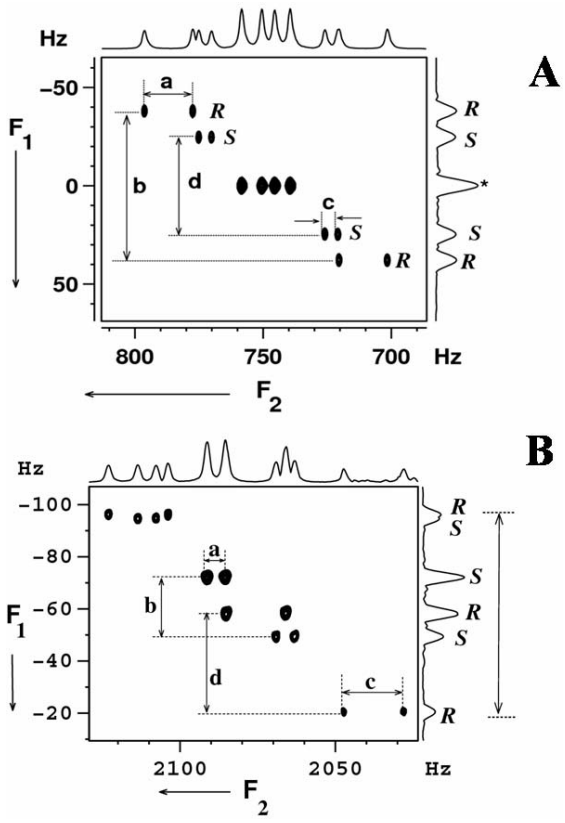

Fig. 26. This renders the spin system in the t_1 dimension to be A_3X. The magnitude of ${}^1T_{\rm CH}$ being larger than ${}^2T_{HH}$, a triplet of a doublet is detected in the t_1 dimension. The two such distinct triplets of doublets discriminates R and$S$ enantiomers unambiguously. The analysis of the spectrum provides ${}^nT_{ij}$, where the superscript n refers to interacting spins i and j that are n bonds away. The separation between the adjacent transitions of the triplet provides ${}^2T_{HH}$ ($3D_{HH}$). This is marked as c and f in the figure for R and$S$ enantiomers respectively. The spectrum in the direct dimension corresponds to the spin system of the type A_3MX, which is a doublet of doublet of a triplet. The methyl protons in the direct dimension experience three different couplings, viz., among themselves (${}^2T_{HH}$), to methine proton (${}^3T_{HH}$) and to ^{13}C of methyl group (${}^1T_{\rm CH}$). The correlated peaks appear tilted due to the presence of ${}^2T_{HH}$ and ${}^1T_{\rm CH}$ in both the dimensions. The cross section taken parallel to the t_2 dimension provides $({}^3T_{HH})^{R/S}$. The analysis of the spectrum corresponding to either $|{}^{13}C_\alpha\rangle$ or $|{}^{13}C_\beta\rangle$ spin states provides all homonuclear couplings. The separations marked a and c in the Fig. 26 provide ${}^3T_{HH}$ and ${}^2T_{HH}$ respectively for R enantiomer. The corresponding parameters for S enantiomer are marked d and f respectively. The displacement between two cross sections of $|{}^{13}C_\alpha\rangle$ and $|{}^{13}C_\beta>$ spin states provides $({}^1T_{\rm CH})^{R/S}$ and are marked b and e respectively.

The methyl selective SERF 2D spectrum is reported in Fig. 27A. Though ${}^2T_{HH}$ are different for the enantiomers, the central peaks of the two triplets resonating at the zero frequency are overlapped due to negligible difference in their chemical shift anisotropies. In the CH-SERF experiment, as a consequence of the introduction of ${}^1T_{\rm CH}$ as an additional parameter with their significantly different values, there is complete discrimination of enantiomers. This is evident from comparison of the $|{}^{13}C_\alpha\rangle$ region of the CH-SERF and conventional SERF spectra reported in Fig. 27B.

The CH-SERF experiment has also been carried out on methine proton. The application of a biselective 180° pulse on methine and methyl protons enabled the evolution of its magnetization under ${}^3T_{HH}$ coupling. The corresponding CH-SERF and SERF spectra are reported in Figs. 28A and 28B respectively. The evolution of ${}^3T_{HH}$ and ${}^1T_{\rm CH}$ in the F_1 dimension results in a quartet of a doublet for each enantiomer. Each component of the doublet with larger separation (${}^1T_{\rm CH}$) is further split into a quartet (${}^3T_{HH}$). The complete discrimination is evident from the tilted broken line joining the four transitions of each enantiomer reported in Fig. 28C. The method has also been applied for the analysis of CH-SERF spectrum of (R/S)-Propylene carbonate, which forms an A_3MPKX, where X is ^{13}C spin coupled to methyl protons and the remaining spins are protons.

11.1.3. *Analyses of CH-DQSERF spectra of (R/S)-3-butyn-2-ol*

For the experimental demonstration of CH-DQSERF (R/S)-3-butyn-2-ol has been chosen. With the inclusion of the ^{13}C spin coupled to methyl protons, the spin system of this molecule corresponds to A_3MPX. The pulse sequence given in Fig. 25B has been employed for CH-DQSERF experiment. The selectively methyl group excited CH-DQSERF spectrum is given in Fig. 29A. The spin system A_3X in the t_1 dimension mimics an AMX type where A is a super spin composed of two protons (active spins) taking part in DQ coherence and M is a passive proton not involved in

Figure 28: (A) The 500 MHz methine proton (H5) excited CH-SERF spectrum of (R/S)-2-chloropropanoic acid in PBLG. The optimized τ delay is 2.08 ms. The seduced shape pulse lengths are 7.14 ms for 90° and 180° selective pulses with rf power optimized accordingly. The 2D data matrix is 720 and 164 points in F_2 and F_1dimensions respectively. Spectral widths of 200 Hz and 190 Hz were chosen in the direct and indirect dimensions respectively. The number of accumulations was 32 for each t_1 increment. Relaxation delay used was 2.5 s. The time domain data was processed by zero filling it to 2k and 1k points in F_2 and F_1 dimensions respectively, with sine square bell window function and without linear prediction. The spectrum has been displayed in magnitude mode with a digital resolution of 0.29 Hz and 0.48 Hz in the direct and indirect dimensions respectively. $|^{13}C_\alpha\rangle$ and $|^{13}C_\beta\rangle$ regions are marked in the F_1 dimension. (B) ^{12}C detected 500 MHz methine proton (H5) excited SERF spectrum of (R/S)-2-chloropropanoic acid in PBLG. (C) The expanded region of Fig. 28A depicted in rectangle. The quartet peaks for each enantiomer is marked with a tilted line joining the peaks. The separations providing the magnitudes of the couplings and their values (in Hz) are; $a = (^1T_{CH})^R = 107.7$, $b = (^1T_{CH})^S = 104.5$, $c = (^3T_{HH})^R = 14.4$ and $d = (^3T_{HH})^S = 10.8$.

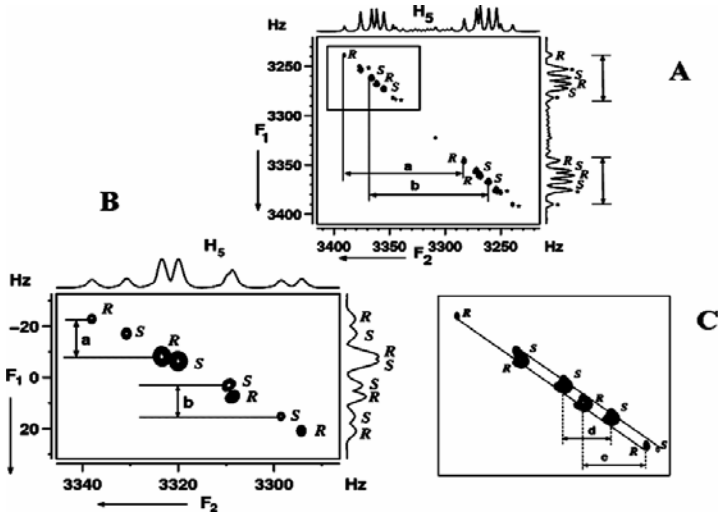

the DQ coherence and X is the ^{13}C spin coupled to methyl protons. A part of AMX is detected in the DQ dimension. Thus the multiplicity pattern in the t_1 dimension is a doublet of a doublet for each enantiomer corresponding to four possible spin states of M and X. The doublet separations marked 'g' and 'h' corresponds to the sum of passive couplings $2(^2T_{HH})$ for *R* and *S* enantiomers respectively. Similarly the doublet separations marked 'p' and 'l' corresponds to the sum of passive couplings $2(^1T_{CH})$ for *R* and *S* enantiomers respectively. Interestingly in this specific example $^1T_{CH}$ is smaller than $^2T_{HH}$, hence there is no isolated groups of transitions pertaining to spin states $|\alpha\rangle$ and $|\beta\rangle$ of ^{13}C, unlike in CH-SERF spectra of the molecules discussed previously.

In the direct dimension spin system corresponds to A_3MPX and displays all the couplings. The spectral pattern for the CH-DQSERF experiment appears different from CH-SERF experiment. This is the consequence of the DQ excitation in the preparation period and the presence of the mixing pulse (i.e. DQ-SQ conversion pulse) at the end of t_1 dimension. The SQ cross section for each transition in the DQ dimension gives rise to enantio pure proton spectrum edited by ^{13}C spin of the methyl group. The cross section for *R* and *S* enantiomers provides the parameters, $^2T_{HH}$, $^3T_{HH}$,$^5T_{HH}$. The $^1T_{CH}$ appears as a displacement between the two cross sections. Thus all the couplings experienced by methyl protons could be extracted from the direct dimension. For comparison, DQSERF spectrum of this molecule is given in Fig. 29C. From the t_2 dimension of this spectrum only one coupling is derivable for the *S* enantiomer. As a result of routing the magnetization through ^{13}C and invoking $^1T_{CH}$ in CH-DQSERF, all the three couplings could be determined as shown in expanded region of the spectrum (Fig. 29B).

11.2. ^{13}*C-edited triple quantum resolved technique*

In the previous sections the two dimensional resolved techniques involving natural abundant ^{13}C as a spy nucleus were discussed. In the present section a triple quantum correlation technique employing ^{13}C is discussed. Before describing the application of this methodology the evolution of

Figure 29: (A) The 500 MHz ^{1}H 2D CH-DQSERF spectrum of (R/S)-3-butyn-2-ol in the chiral liquid crystal solution of PBLG in the solvent $CDCl_3$ along with F_1 and F_2 projections. All the peaks of 2D projection in the direct dimension could be correlated to the peaks in R and S enantiomer cross sections. Peaks marked * are of low intensity and can be seen in the magnified scale. (B) Expanded region of a narrow strip marked with broken rectangle corresponding to S enantiomer and (C) The 500 MHz ^{1}H 2D DQSERF spectrum of the molecule with F_1 and F_2 projections. A cross section for S enantiomer is expanded in the box below. The $({}^nT_{HH})^{R/S}$ are obtained from the marked separations. These values in Hz are; The values of the parameters (in Hz) are; $a = ({}^1T_{CH})^R = 78.4$, $g = 2({}^2T_{HH})^R = 210.4$, $b = ({}^5T_{HH})^R = 9.8$, $c = ({}^3T_{HH})^R = 36.1$, $d = ({}^2T_{HH})^R = 105.2$ Hz, $e = ({}^1T_{CH})^S = 106.5$, $h = {}^2(2T_{HH})^S = 93.8$, $f = ({}^5T_{HH})^S = 8.9$, $j = ({}^2T_{HH})^S = 46.9$ and $i = ({}^3T_{HH})^S = 36.1$, $l = 2({}^1T_{CH})^R = 156.8$ and $q = 2({}^1T_{CH})^S = 213.0$.

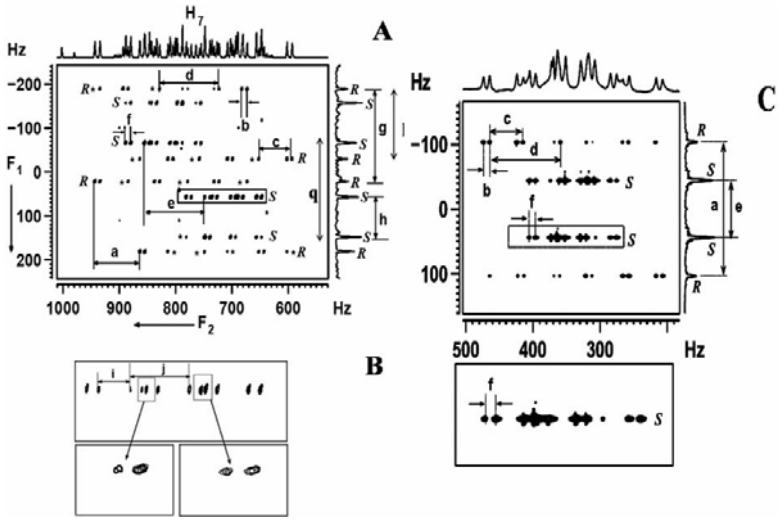

magnetization during the developed pulse sequence is discussed.

11.2.1. *Theoretical description of the pulse sequence*

The pulse sequence developed for this methodology[66] is reported in Fig. 30. The evolution of magnetization at different time points of the pulse sequence is easily understood by the product operator formalism[34]. The pulses with rectangular shapes are non-selective while the remaining pulses are spin selective. The pulse sequence starts with polarization transfer via INEPT block. At the end of delay τ^* the antiphase ^{1}H magnetization is converted into longitudinal two spin-orders by the 90° ^{1}H pulse applied along the y axis at time point A. At this stage application of a homospoil gradient pulse eliminates undesired coherences and following this the two spin-orders is back converted into the antiphase proton magnetization of the methyl group by the selective 90° pulse on methyl protons at time point C via the anti phase coherence of ^{13}C spins. From the point C to D the magnetization is allowed to evolve under D_{HH} among methyl protons by a selective refocusing pulse which also decouples this group from the passive protons and the ^{13}C spin. At the time point D there is doubly anti phase magnetization with respect to protons, i.e., $I_{1Y}I_{2Z}I_{3Z}S_{2Z}$. The application of a selective 90^0 pulse of phase y on methyl resonance converts this into $I_{1Y}I_{2X}I_{3X}S_{2Z}$, the homonuclear multiple quantum terms at time point D. The 3Q coherence is selected by a suitable gradient ratio and allowed to evolve under the sum of different homonuclear and heteronuclear passive couplings, by the non-selective refocusing pulse on ^{13}C and ^{1}H in the middle

Figure 30: The pulse sequence for spin selective 3Q-SQ correlation of methyl protons edited by ^{13}C spin. The A, B, C, D and E are the markings to discuss the behaviour of the magnetization during different stages of pulse sequences. Rectangular pulses are hard pulses. All the remaining pulses are spin selective. The phases of pulses are; Φ_1 = x, Φ_2 = x x x x -x –x -x -x, Φ_3 = (12) x, Φ_4 = y, Φ_5 = x -x x -x x -x x -x, Φ_6 = y, Φ_7 = x x y y -x -x -y -y, Φ_8 = (12) -y, Φ_9 = x x x x x x x x -x -x -x -x -x -x -x -x, Φ_R= x -x -x x x -x -x x -x x x -x -x x x –x.

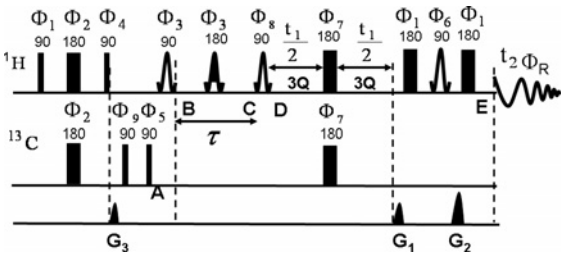

Figure 31: Selective ^{13}C edited methyl protons excited 2D 3Q-SQ correlated spectrum of (*R*/*S*)-3-butyn-2-ol along with the corresponding projections. The optimized τ delay is 10 ms. The seduced shape pulse lengths are 4.16 ms and 6.9 ms for 90° and 180° selective pulses respectively with rf power optimized accordingly. The 2D data matrix is 1.3 k and 384 points in F_2 (SQ) and F_1 (3Q) dimensions respectively. Spectral widths of 600 Hz and 500 Hz were chosen in the direct and indirect dimensions respectively. The number of accumulations was sixteen for each t_1 increment. Relaxation delay used was 4 s. The time domain data was processed by zero filling it to 2 k and 1 k points in F_2 and F_1 dimensions respectively, with sine square bell window function and with linear prediction to 512 points, to obtain high resolution and undistorted baseline, in the F_1 dimension. The spectrum has been displayed in magnitude mode with a digital resolution of 0.29 Hz and 0.48 Hz in the direct and indirect dimensions respectively. F_1 dimension pertains to 3Q spectrum. $\alpha(^{13}C)$ and $\beta(^{13}C)$ regions are marked in the F_1 dimension. The assignments to *R* and *S* transitions are marked. The * marks represent transitions of low intensities.

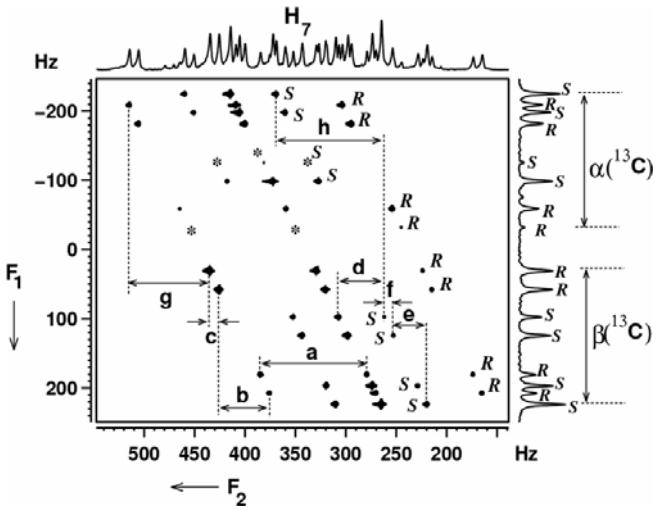

of the 3Q evolution period. This also overcomes the problem of field inhomogeneity encountered in the 3Q coherence, thereby providing higher resolution. The last selective 90°y pulse on methyl protons results in the observable SQ magnetization in the direct dimension at time point F. The INEPT transfer edits the ^{1}H magnetization by ^{13}C spin states and also improves the overall sensitivity.

The 3Q exorcycle phase cycling has been employed for non-selective 180^0 pulse in the middle of t_1 dimension. Double isotope filtration phase cycling has been applied for the phases Φ_9 and Φ_5. During the excitation of 3Q coherence and its evolution and conversion to SQ coherence, the spin states of the remaining protons (passive spins) in the molecule and ^{13}C spin of the methyl group are undisturbed in both the dimensions. This enables the detection of SQ transitions of the methyl protons (A_3 spin system) based on the spin states of the passive ^{1}H and ^{13}C spins and exploits all the advantages of the sequence discussed earlier.

11.2.2. *The interpretation of ^{13}C edited 3Q-SQ spectrum of (R/S)-3-butyn-2-ol*

Considering that one percent of the molecules have protons of the methyl group attached to ^{13}C, the spin system of this molecule can be considered to be of the type A_3MPX where A refers to methyl protons, M and P corresponds to methine and acetylenic protons and X is the ^{13}C spin attached to methyl group. As discussed previously when the magnetization is not routed through ^{13}C spin, there are 12 transitions for the methyl protons for each enantiomer. When ^{13}C is a participating spin there are 24 transitions for each enantiomer, which can be visualized as eight sub spectra according to eight possible spin states of M, P and X spins. The designed pulse scheme separates all the eight sub spectra from each other, and detects them independently in well separated arrays of SQ dimension. The anisotropic proton chemical shift difference between the two enantiomers is negligibly small and hence the two sets of peaks arising from both *R* and *S* enantiomers are overlapped for the ^{12}C bound one dimensional ^{1}H spectra as well as the ^{13}C bound satellite proton spectra.

The ^{13}C edited methyl protons excited 3Q-SQ spectrum is shown in Fig. 31. The selective excitation of 3Q coherence of the methyl protons results in the simultaneous flipping of all the protons. However, the non-selective refocusing pulse on ^{13}C and ^{1}H leads to refocusing of chemical shift evolution and retention of passive heteronuclear and homonuclear couplings. Thus the spin system in the 3Q dimension will be of the type AMPX, where A is the super spin with three methyl protons. The 3Q dimension will be an A part of this AMPX type spin system. The spectrum in the SQ dimension is the ^{13}C satellite proton spectrum with the suppression of peaks from ^{12}C attached protons. The connectivity of 3Q-SQ direct peaks forms a distinct pattern for each enantiomer in the 2D spectrum which unambiguously discriminate the enantiomers.

In the 3Q dimension, the largest coupling to spin A arises due to $J_{CH}+2D_{CH}$, where J_{CH} and D_{CH} are the scalar and the dipolar couplings between proton and ^{13}C of the methyl group. In the spin product basis set the 3Q states of proton are $|\alpha_A\alpha_A\alpha_A\rangle$ and $|\beta_A\beta_A\beta_A\rangle$. This is coupled to spin states $|\alpha\rangle$ and $|\beta\rangle$ of ^{13}C spin. Hence the resonance of spin A is split into a doublet. Two such doublets are expected, one for each enantiomer. The value of D_{CH} being different for both the enantiomers and scaling of the $(J_{CH}+2D_{CH})$ by a factor of three resulted in enhanced spectral resolution and

Figure 32: (a–h) The cross sections taken along F_2 dimension for each sub spectrum edited by passive spin states in Fig. 31, plotted with same horizontal scale for comparison. Only the cross sections pertaining to $\beta(^{13}C)$ regions are given. *R* and *S* assignments and the passive proton spin states in the 3Q dimension are shown.

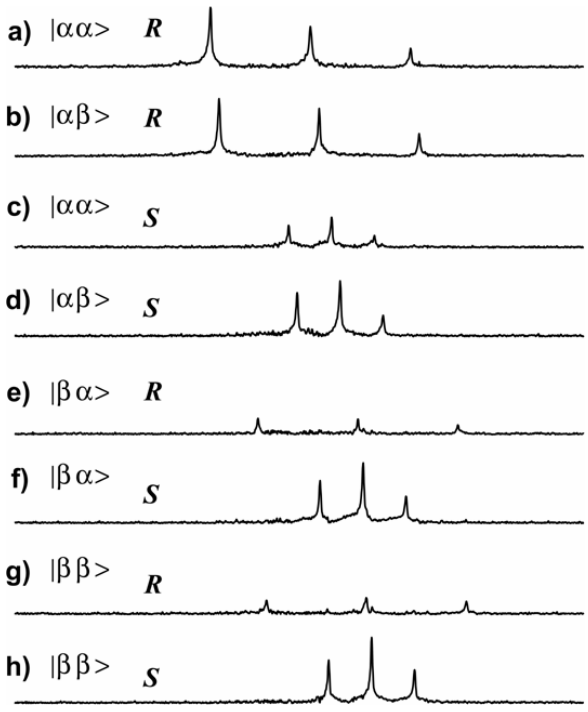

unambiguous enantiomer visualization. This also can be construed as the separation of ^{13}C satellites in the one dimensional spectrum. The two 3Q transitions edited by the ^{13}C spin states are further split by the remaining two methine and acetylenic protons into four transitions according to their four spin states $|\alpha_M\alpha_P\rangle$, $|\alpha_M\beta_P\rangle$, $|\beta_M\alpha_P\rangle$ and $|\beta_M\beta_P\rangle$. Thus a total of eight 3Q transitions are observed for each enantiomer. Four of them correspond to $|\alpha\rangle$ state of ^{13}C while another four correspond to $|\beta\rangle$ state.

The 3Q transitions corresponding to $|\alpha\rangle$ and $|\beta\rangle$ domains of ^{13}C are marked as $\alpha(^{13}C)$ and $\beta(^{13}C)$ as shown in Fig. 31. Chiral discrimination is obvious from the highly resolved 3Q spectrum in the F_1 dimension. The sub spectral analysis at any one of the ^{13}C spin states provides the coupling of methyl protons to all the passive protons. The different displacement vectors g and h, b and e, c and f between sub spectra drawn in Fig. 31 provides passive coupling parameters $J_{CH}+2D_{CH}$, $^3T_{HH}$ and $^5T_{HH}$ for the enantiomers. The separations marked a and d in the Fig. 31 provides $^2T_{HH}$ for the *R* and *S* enantiomers respectively.

The cross sections taken along the SQ dimension at different passive proton spin states of 3Q dimension for the $\beta(^{13}C)$ region are plotted in Fig. 32. Each of these cross sections pertains to selectively detected SQ transitions originating from the 3Q transition whose initial and final states have the same passive spin state. An example of such a SQ transition is from the state $|\alpha_A\alpha_A\alpha_A\beta_M\beta_P\beta_X\rangle$ to $|\beta_A\alpha_A\alpha_A\beta_M\beta_P\beta_X\rangle$ which arises from a 3Q transition like $|\alpha_A\alpha_A\alpha_A\beta_M\beta_P\beta_X\rangle$ to $|\beta_A\beta_A\beta_A\beta_M\beta_P\beta_X\rangle$ where the initial and final passive spin states are $|\beta_M\beta_P\beta_X\rangle$. Thus all the proton SQ transitions pertaining to eight A_3 sub spectra get separated into different cross sections depending on the spin states of the passive spins. Also each cross section is a triplet, from which D_{HH} among methyl protons can be determined. The distinct two sets of triplets differentiates the enantiomers.

A comparison of the 3Q-SQ correlation for ^{12}C attached protons and ^{13}C attached protons is shown in Fig. 33. The isolated $\beta(^{13}C)$ region is plotted separately in the expanded scale for comparison. The 3Q-SQ correlation of ^{12}C attached protons leads to spin state selection by only passive proton spins and discriminate twenty out of the twenty four transitions. However, the transitions marked with star are the overlap of two transitions from the two enantiomers. The 3Q-SQ correlation of ^{13}C attached protons discriminate all the twenty four transitions, a consequence of additional spin state selection by the ^{13}C spin.

11.2.3. *The ^{13}C edited 3Q-SQ spectrum of (R/S)-propylene carbonate*

The protons and the carbon attached to methyl group of this molecule form a weakly coupled spin system of the type A_3MNPX where A_3 corresponds to active methyl protons, M and N are the two methylene protons, P is the methine proton and X is the ^{13}C spin. The methyl protons experience five different types of couplings, viz. (a) the couplings among themselves ($^2T_{HH}$), (b) the coupling between methyl and methine (P) protons ($^3T_{HH}$), (c) the two different couplings from the two diastereomeric methylene (M and N) protons ($^4T_{HH}$) and (d) the coupling from the ^{13}C spin (X). The first order analysis indicate that there are forty eight transitions for each enantiomer, which can be visualized as sixteen A_3sub spectra corresponding to sixteen passive spin states of M, N, P and X together. Thus there are total of 96 overlapped transitions from both the enantiomers. The separation and identification of these transitions is a challenging task.

Figure 33: (a) ^{12}C attached methyl protons excited 2D 3Q-SQ correlated spectrum of (*R*/*S*)-3-butyn-2-ol in the liquid crystal solvent PBLG. The 2D data matrix is 1228 X 336 and zero filled to 4 k and 1 k before processing. The sine bell window function has been used in both the dimensions. Four scans for each FID and a recycle delay of 7 s. The optimized τ delay is 10 ms. The seduce shaped pulse lengths are 6.25 ms for both 90° and 180° pulses with different power levels. Digital resolution is 0.5 Hz and 0.1 Hz in F_1 and F_2 dimensions. Assignments of spin state selected sub spectrum to *R* and *S* enantiomers are shown. The $*$ marks indicate the overlap of two transitions from *R* and *S*. The separations a, b and c marked provide $^2T_{HH}$, $^3T_{HH}$ and $^5T_{HH}$ for *R* enantiomer and those marked with d, e and f provide the similar information for *S* enantiomer; (b) ^{13}C edited methyl protons excited 2D 3Q-SQ correlated spectrum of (*R*/*S*)-3-butyn-2-ol. Only $\beta(^{13}C)$ region of Fig. 31 is plotted in expanded scale. Assignments of spin state selected sub spectrum to *R* and *S* enantiomers are shown. Note the advantage of spin state selection in the discrimination of even the peaks marked with $*$ of Fig.33a.

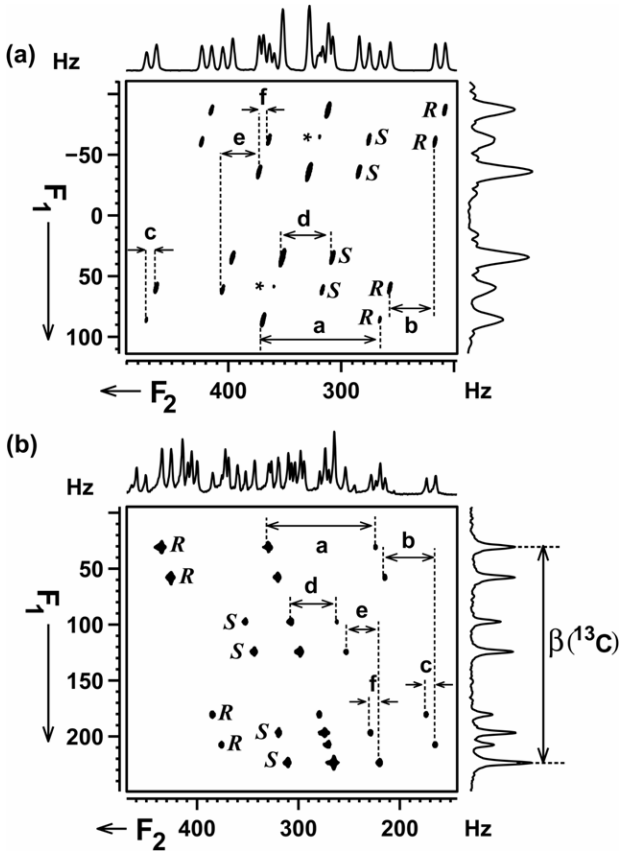

The selective methyl protons excited, ^{13}C edited 2D 3Q-SQ correlation spectrum of (*R*/*S*)-propylene carbonate is given in Fig. 34. In the 3Q dimension, the spin system is of the type AMNPX. The super spin A is the three methyl protons (the active spin), the methine and methylene protons (M, N and P) and one ^{13}C spin (X) constitute the passive spins. The $^2T_{HH}$ in A_3 is the active coupling while one $^3T_{HH}$ and two $^4T_{HH}$ along with heteronuclear $^1T_{CH}$constitute the passive couplings. The 3Q dimension provides sixteen transitions for each enantiomer pertaining to sixteen spin states of M, N, P and X. The displacements between the SQ transitions corresponding to $|\alpha\rangle$ and $\beta\rangle$ domains of ^{13}C marked 'a' and 'f' are the passive heteronuclear coupling $^1T_{CH}$ for the *R* and *S* enantiomers respectively.

The analyses of the spectra at any one of the spin states of ^{13}C is sufficient to derive all the homonuclear couplings with methyl protons. For the *S* enantiomer the two types of $^4T_{HH}$ are equal and hence results in a triplet of a doublet (due to $^3T_{HH}$) in the 3Q dimension and are marked *S*. However, for the *R* enantiomer the two types of $^4T_{HH}$ are unequal. Hence 3Q dimension provides eight distinct transitions marked *R* in the figure.

For clarity the expanded $\alpha(^{13}C)$ region is also given in Fig. 34B. The alphabets marked 'b' and 'g' denote the active coupling, $^2T_{HH}$ responsible for the triplet (sub spectrum) in each SQ cross section, for the *S* and *R* enantiomers respectively. Thus each cross section taken along the SQ dimension for each passive spin state in 3Q dimension is a triplet. The eight A_3 sub spectra (triplets) for eight passive spin states are observed for *S* enantiomer. However, for *R* enantiomer, six triplets with smaller dipolar couplings are observed. The passive homonuclear couplings are determined from the displacements marked c, d, e and h, i, j for the *S* and *R* enantiomers respectively. It may be pointed out that the coupling information among protons numbered, 5, 6 and 7 is not reflected either in the 3Q or in the SQ dimension. In addition to all the advantages of the method described previously, additionally D_{CH} can be derived.

12. Conclusions

In this review we have provided extensive discussion our recently developed methods for the visualization and the analyses of the proton NMR spectra of chiral molecules. The origin of the complexity of proton NMR spectra and the difficulties encountered in their analyses has been demonstrated. The novel experimental techniques have been developed by manipulating the spin dynamics in overcoming some of these problems. The developed experimental methodologies employ single quantum one dimensional correlation technique, two dimensional correlation and resolved techniques, the spin selective and non-selective multiple quantum excitation. These developed methodologies employ proton NMR detection for discrimination, the separation of the overlapped spectra of enantiomers and discerning

Figure 34: A) The ^{13}C edited selective methyl protons excited 2D 3Q-SQ correlated spectrum of (*R*/*S*)-propylene carbonate along with the corresponding projections. The optimized τ delay is 25 ms. The seduced shape pulse lengths are 3.125 and 3.7 ms for 90° and 180° pulses respectively. The 2D data matrix of 800 and 576 points in F_2 (SQ) and F_1 (triple quantum) dimensions respectively, were chosen. Spectral widths of 535 Hz and 300 Hz were chosen in the direct and indirect dimensions respectively. The number of accumulations was twenty four for each t_1 increment. Relaxation delay used was 3 s. The time domain data was processed by zero filling it to 2 k and 1 k points in F_2 and F_1 dimensions respectively, with sine bell window function and without linear prediction. The spectrum has been displayed in magnitude mode with digital resolutions of 0.15 Hz and 0.52 Hz in the direct and indirect dimensions respectively. F_1 dimension pertains to 3Q spectrum. $\alpha(^{13}C)$ and $\beta(^{13}C)$ regions are marked in the F_1 dimension. The assignment of peaks to *R* and *S* marked and also shown with tilted arrows. The displacements of $\alpha(^{13}C)$ and $\beta(^{13}C)$ regions in the F_2 dimension providing heteronuclear passive couplings are marked as a and f for *S* and *R* enantiomers respectively. Peaks with very low intensities are marked with ∗; (B) The expanded $\alpha(^{13}C)$ region of Fig. 34A. The separations marked with alphabets b - e and g - j provide proton-proton coupling information and the corresponding values are reported in table 1. Assignments to the enantiomer peaks are marked.

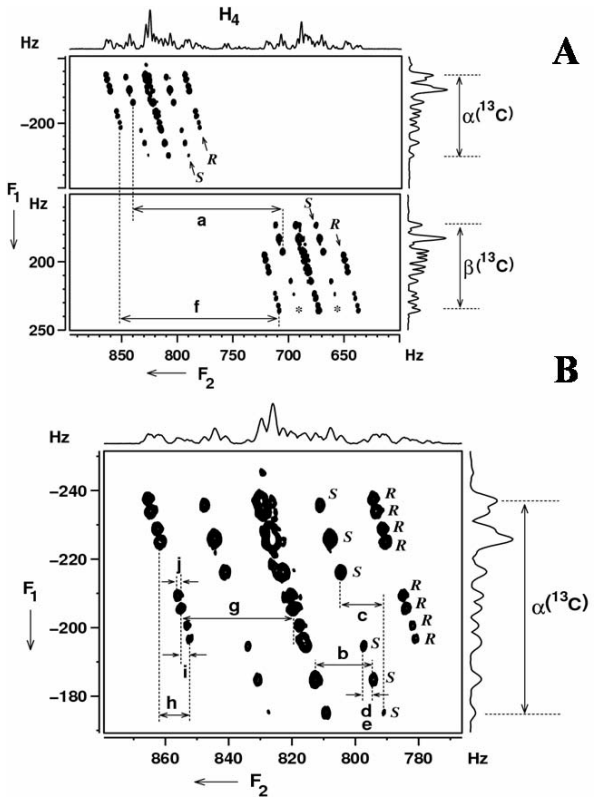

the degenerate transitions from the broad and featureless one dimensional spectra of chiral molecules. The utilization of natural abundant ^{13}C as a spy nucleus aided further spectral simplification and enantiomer differentiation. All the experimental pulse sequences have been discussed taking specific examples. The routine application of ^{1}H NMR for visualization of enantiomers, which was hitherto reported in the literature as difficult or impossible, has been demonstrated to be possible. The feasibility of the methods for the precise determination of enantiomeric excess has also been discussed.

13. Acknowledgements

NS gratefully acknowledges the financial support by Board of Research in Nuclear Studies, New Delhi for the research grant no. SR/S1/PC-32/2008. URP and NN would like to thank CSIR for senior research fellowship.

Received 16 October 2009; accepted 28 October 2009.

References

1. Kalsi, P. S. (2005) Stereochemistry, Conformation and Mechanism, New Age International Pvt Ltd, New Delhi.
2. Rinaldi, P. L. (1982) Prog Nucl Magn Reson Spectrosc 15, 291.
3. Fraser, R. R. (1982) In Assymmetric Synthesis, Academic Press: New York 1, 173.
4. Morrill, T. C. (1986) Methods in Stereochemical Analysis; Ed. VCH Publishers Inc.: New York.
5. Weisman, G. R. (1983) In Asymmetric Synthesis, Academic Press: New York 1, 153.
6. Pirkle, W. H., Hoover, D.J. (1982) Top Stereochem 13, 263.
7. Yamaguchi, S. (1983) In Asymmetric Synthesis, Ed. Morrison, J.D., Academic Press: New York, 1, 125.
8. Sackmann, E. E., Meiboom, S., Snyder, L. C. (1968) J Am Chem Soc 90, 2183.
9. Sarfati, M., Lesot, P., Merlet, D., Courtieu, J. (2000) Chem Commun 2069.
10. Lesot, P., Gounelle, Y., Merlet, D., Lowensteinand, Courtieu, J. (1995) J Phys Chem 99, 14871.
11. Lafontaine, E., Bayle, J. P., Courtieu, J. (1989) J Am Chem Soc 111, 8294 .
12. Elliot, A., Ambrose, E. J. (1950) Discuss Faraday Soc 9, 246.
13. Robinson, C. (1956) Trans Faraday Soc 52, 571.
14. Robinson, C. (1966) Mol Cryst Liq Cryst 1, 467.
15. Czarniecka, K., Samulki, E. T. (1981) Mol Cryst Liq Cryst 63, 205.
16. Doty, P., Bradbury, J. H., Holtzer, A. M. (1956) J Am Chem Soc 78, 947.
17. Pauling, L., Corey, R. B., Brandson, H. R. R. (1951) Prog Nucl Magn Reson Spectrosc 37, 205.
18. Panar, M., Phillips, W. D. (1968) J Am Chem Soc 90, 3880.
19. Samulski, E. T., Tobolsky, A. V. (1968) Macromolecules 1, 555.
20. Mitchell, J. C., Woodward, A. E., Doty, P. (1957) J Am Chem Soc 79, 3955.
21. Merlet, D., Ancian, B., Courtieu, J., Lesot, P. (1999) J Am Chem Soc 121, 5249.
22. Canet, I., Courtieu, J., Loewenstein, A., Meddour, A., Péchiné, J. M. (1995) J Am Chem Soc 117,6520.
23. Canet, I., Meddour, A., Courtieu, J., Canet, J. L., Salaün, J. (1994) J Am Chem Soc 116, 2155.
24. Smadja, W., Auffret, S., Berdagué, P., Merlet, D., Canlet, C., Courtieu, J., Legros, J. Y., Boutros, A., Fiaud, J. C. (1997) Chem Commun 2031.
25. Lesot, P., Courtieu, J. (2009) Prog. Nucl. Magn. Reson. Spect. 55, 128.
26. Nath, N., Suryaprakash, N. (2009) J Magn Reson 202, 34–37 (2010).
27. Keeler, J. (2005) Understanding NMR Spectroscopy, John Wiley and Sons, England.
28. Farjon, J., Merlet, D., Lesot, P., Courtieu, J. (2002) J Magn Reson 158, 169.
29. Fäcke, T., Berger, S. (1995) J Magn Reson A 113, 114.
30. Farjon, J., Baltaze, J. P., Lesot, P., Merlet, D., Courtieu, J. (2004) Magn Reson Chem 42, 594.

31. Bikash, B., Prabhu, U. R., Suryaprakash, N. (2008) J Phys Chem B 111, 12403.
32. Pople, J. A., Schneider, W. G., Bernstein, H.J. (1959) High Resolution Nuclear Magnetic Resonance, McGraw Hill: New York.
33. Norwood, T. J. (1992) Prog Nucl. Magn Reson Spect 24, 295.
34. Sørensen, O. W., Eich, G. W., Levitt, M. H., Bodenhausen, G., Ernst, R. R. (1983)) Prog Nucl Magn Reson Spect 16, 163.
35. Emsley, L. (1994) Methods in Enzymology 239, 207.
36. Griesinger, C., Sørensen, O. W., Ernst, R. R. J Am Chem Soc 107 2985.
37. Griesinger, C., Sørensen, O. W., Ernst, R. R. (1986) J Chem Phys 85, 6837.
38. Uday, R. P., Bikash, B., Suryaprakash, N. (2008) Phy. Chem A 112, 5658.
39. Uday, R. P., Suryaprakash, N. (2008) J Magn Reson 195, 145.
40. Brüschweiler, R., Griesinger, C., Sørensen, O. W., Ernst, R. R. (1988) J Mag Reson 78, 178.
41. Bax, A., Freeman, R. (1981) J Magn Reson 44, 542.
42. Brüschweiler, R., Madsen, J. C., Griesinger, C., Sørensen, O. W. Ernst, R. R. (1987) J Magn Reson 73, 380.
43. Emsley, L., Bodenhausen, G. (1989) J Magn Reson 82, 211.
44. Cavanagh, J., Waltho, J. P., Keeler, J. (1987) J Magn Reson 74, 386.
45. Beguin, L., Courtieu, J., Ziani, L., Merlet, D. (2006) Magn Reson Chem 44, 1096.
46. Beguin, L., Giraud, N., Ouvrard, J. M., Courtieu, J., Merlet, D. (2009) J Magn Reson 119, 41.
47. Oschkinat, H., Pastore, Pfändler, P., Bodenhausen, G. (1986) J Magn Reson 69, 559.
48. Uday, R. P., Suryaprakash, N. (2009) J Magn Reson 202, 217–222 (2010).
49. Pell, A.J., Edden, R. A. E., Keeler, J. (2007) Magn Reson Chem 45, 296.
50. Pfändler, P., Bodenhausen, G. (1986) J Magn Reson 70, 71.
51. Rani, G. C. R., Suryaprakash, N., Kumar, A., Khetrapal, C. L. (1994) J Magn Reson A 107, 79.
52. Rani, G. C. R., Suryaprakash, N. (2000) In New Advances in Analytical Techniques, Ed. Atta-ur-Rahman, Harwood Academic Press:The Netherlands 1, 441.
53. Pfändler, P., Bodenhausen, G. (1991) J Magn Reson 91, 65.
54. Oschkinat, H., Clore, G. M., Nilges, M., Gronenborn, A. M. (1987) J Magn Reson 75, 534.
55. Thrippleton, M. J., Keeler, J., (2003) Angew Chem Int Ed 42, 3938.
56. Eggenberger, U., Pfändler, P., Bodenhausen, G. (1988) J Magn Reson 77, 192.
57. Jeannerat, D., Ronan, D., Baudry, Y., Pinto, A., Saulnier, J. P., Matile, S. (2004) Helv Chim Acta 87, 2190.
58. Turner, C. J. (1992) J Magn Reson 100, 483.
59. Marathias, V. M., Tawa, G. J., Goljer, I., Bach, A. C. (2007) Chirality 19, 741.
60. Bikash, B., Uday, R. P., Suryaprakash, N. (2008) J Magn Reson 192, 101.
61. Uday, R. P., Bikash, B., Suryaprakash, N. (2008) J Magn Reson 191, 259.
62. Morris, G. A., Freeman, R. (1979) J Am Chem Soc 101, 760.
63. Kobzar, K., Kessler, H., Luy, B. (2005) Angew Chem Int Ed 44, 3145.
64. Ziani, L., Courtieu, J., Merlet, D. (2006) J Magn Reson 183, 60.
65. Nath, N., Baishya, B., Suryaprakash, N. (2009) J Magn Reson 200, 101.
66. Bikash, B., Uday, R. P. and Suryaprakash, N. (2008) J Magn Reson 192, 92.

Uday R. Prabhu. b. 1981. M.Sc. 2003, Chemistry, Karnatak University Dharwad. Currently doing graduate studies at the NMR Research Center, Indian Institute of Science, Bangalore. Research interests include Chiral discrimination of organic molecules dissolved in chiral liquid crystal using one and two dimensional 1H NMR spectrum.

Sankeerth Hebbar received his M.Sc. degree in Materials Science from Mangalore University. He is currently a PhD student at the Indian Institute of Science, Bangalore. His ongoing Ph.D.studies are on the development and applications of Multiple Quantum NMR.

N. Suryaprakash, Ph.D. 1986, Bangalore University, Bangalore (supervisors Prof. C.L. Khetrapal and Prof. G.K. Narayana Reddy), Postdoctoral research at University of Basel, Switzerland, 1990–91 (Prof. Peter Diehl), Ben Gurion University of the Negev, Israel; 1998–1999 (Prof. Raz Jelinek) University of Southampton, United Kingdom 1999–2000 (Prof. J.W. Emsley). Presently Faculty of NMR Research Centre, Indian Institute of Science, Bangalore. Fellow of National Academy of Sciences, Allahabad, India. Research Interests: Development of multi dimensional single quantum and multiple quantum NMR Methodologies. Structures of molecules in the liquid crystalline media, NMR Methods for the study of enantiomers, weak molecular interactions.

Nilamoni Nath obtained his M.Sc. degree in Chemistry with specialization in Inorganic Chemistry in 2007, from Gauhati University, Assam. He is currently a PhD student at the Indian Institute of Science, Bangalore. His research interests are on the development and applications of NMR methodologies for study of chiral drug molecules.